

Dynamical behavior of molecular motor assemblies in the rigid and crossbridge models

T. Guérin^{1,a}, J. Prost^{1,2}, and J.-F. Joanny¹

¹ Physicochimie Curie (Institut Curie/CNRS-UMR168/UPMC), Institut Curie, Centre de Recherche, 26 rue d'Ulm 75248 Paris Cedex 05 France

² ESPCI, 10 rue Vauquelin, 75231 Paris Cedex 05, France

Received 10 March 2011

Published online: 23 June 2011 – © EDP Sciences / Società Italiana di Fisica / Springer-Verlag 2011

Abstract. We present a detailed analysis of the dynamical instabilities appearing in two kinetic theories for the collective behavior of molecular motors: the rigid two-state model and the two-state crossbridge (or power-stroke) model with continuous binding sites. We calculate force-velocity relations, discuss their stability, plot a diagram that summarizes the oscillation regimes, identify the location of the Hopf bifurcation with a memory effect, discuss the oscillation frequency and make a link with single-molecule experiments. We show that the instabilities present in these models naturally translate into non-linearities in force-displacement relations, and at linear order give forces that are similar to the delayed stretch activation observed in oscillating muscles. We also find that instabilities can appear for both apparent load-decelerated and load-accelerated detachment rates in a 3-state crossbridge model.

1 Introduction

Molecular motors are proteins that convert chemical energy into mechanical work to generate motion along and forces on the filaments of the cytoskeleton [1]. In many situations, molecular motors work within groups rather than individually. In a number of examples, groups of motors show a complex dynamical behavior, such as hysteresis, oscillations or bidirectional motion: cardiac myofibrils spontaneously oscillate [2] with a period that correlates with the heartbeat [3,4] even in the absence of the cellular electrical machinery, the wingbeat of asynchronous insect flight muscles is not correlated to the excitatory nervous signal [5]. Non-muscular systems display also dynamic behavior: the beating of flagella and cilia is powered by dynein motors [6], and the mechano-sensory hair-bundles of the vertebrate inner ear spontaneously oscillate in *in vitro* experiments [7], possibly improving the gain and frequency selectivity for sound detection [8]. Even in intracellular transport, cargoes transported by molecular motors can display complex motion [9]: for example, the motion of lipid droplets towards the periphery of *Drosophila* embryos is made of a succession of phases in opposite directions [10] and is therefore bidirectional.

Several theoretical models indicate that these complex behaviors can naturally emerge from collective properties of the molecular motors (see [11–16], and see [17–19] for reviews). These models suggest that, as in many

situations in physics [20], the collective behavior of interacting elements cannot be understood by considering only the behavior of a single isolated molecule. Instabilities, hysteretic effects or oscillations of molecular motor assemblies are observed in *in vitro* experiments with a minimal number of components [21,22], and theories that take into account the collective behavior of motors compare well to many experiments [23–27]. The theories that describe both the internal degrees of freedom of the motors and their collective behavior can be grouped into two main classes: crossbridge power-stroke models [28,13,14] and rigid two-state models [15,12]. In both approaches, the motors act collectively because they are attached to a common rigid backbone: the individual behavior of each motor depends on the velocity of the filament with respect to the backbone, which is itself the result of the combined action of all the motors within the assembly. Both types of models generate instabilities that are linked to the fact that the force exerted by the motors on the filament can amount to a negative friction force at low velocities.

The crossbridge model was first introduced by Huxley in 1957 [28] in order to describe the relation between tension and contraction velocity in muscles. It was realized later that this model could give rise to instabilities in the case where the detachment rates of the motors from their filament depends on the load applied to each motor [13,14]. In crossbridge models, the motors are represented by springs, and the mechanism of force generation is linked to the existence of a conformational change, called the power-stroke, which puts the

^a e-mail: thomas.guerin.2003@polytechnique.org

spring under tension. Conversely, in the rigid two-state model, the motors are represented by particles that interact with the filament *via* a periodic interaction potential [15]. In both theories, the motors can switch between several states, and the energy input is implicitly represented by the fact that the transition rates between the states break the detailed balance condition. Because of the importance of these transition rates, we refer to both types of models as “kinetic models”. As we will see in this paper, these models share many common features. They can also be explicitly related, as they appear as two limiting cases of a more general theory [29].

Although the rigid two-state and crossbridge models are widely used in the literature, they still have not been studied and compared systematically. In this paper, we give a study as complete as possible of both theories, focussing mostly on dynamic instabilities. Biological systems involving molecular motors show spontaneous oscillations with a broad range of frequencies and shapes: oscillations of isolated cardiac muscles are in the range of a few Hz, whereas the wingbeat frequency of some insects is in the range of a few kHz. We discuss the parameters which monitor the oscillations, and the conditions to obtain oscillations with a period smaller than the typical time of the chemical cycle, which lies in the range of 10 ms. We make an explicit link between these oscillations and existing models of stick-slip by identifying the location of the Hopf bifurcation to a memory effect. We investigate the shape of the force-displacement relations and find that non-linearities can emerge as a result of the proximity of a dynamic instability. We also try to relate the models for the collective behavior of molecular motors to the individual properties of motors that can be measured in single-molecule experiments. Finally, we ask whether or not the prediction of these models depend on the precise choice of transition rate functions, and we compare the predictions of the two theories.

The outline of this paper is as follows. We first recall the hypotheses of the rigid two-state model and give a detailed study of this model: we investigate the possible shapes of the force-velocity relation, the regimes of oscillations and the force-displacement relations. Then, we carry out the same study, although with less details, for the crossbridge model: we highlight the similarities and the differences between the two models, and show how to relate the properties of motor assemblies to the results of single-molecule experiments. Finally, we show that the force response to a small displacement step is similar in both models to the delayed stretch activation observed in oscillating muscles.

2 Instabilities in the rigid two-state model

2.1 Hypotheses of the rigid two-state model

We recall here the hypotheses of the rigid two-state model originally introduced in ref. [15]. In this model, the center of mass of each of the N molecular motors is represented

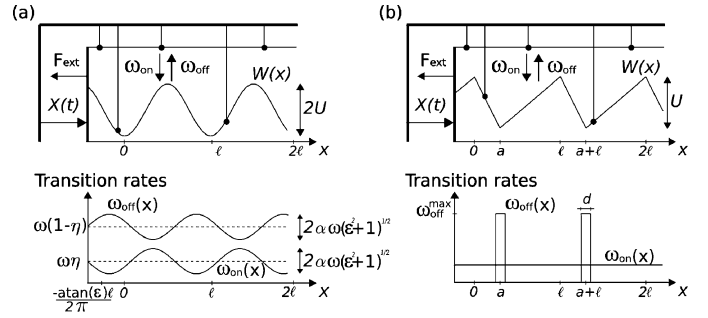


Fig. 1. Sketch of the rigid two-state model, and representation of the two sets of hypotheses studied in the paper. (a) Uniform rate approximation, (b) localized rate approximation.

by a particle rigidly attached to a stiff inextensible backbone (fig. 1). Each particle can be in two states $i = (1, 2)$. In each state i , a motor interacts with the filament through an interaction potential $W_i(x)$, where x is the coordinate of the motor along the filament. As noted in ref. [15], in the limit of an infinite number of motors, only the difference $W(x) = W_2(x) - W_1(x)$ plays a role, we can therefore assume that $W_1(x)$ is uniform without loss of generality. Within this assumption, state 1 is a state where there is no interaction with the filament, that is why we refer to state 1 as the “detached” state (or “weakly bound” state). State 2 is called the “attached” state, where the interaction potential $W(x)$ has a finite amplitude U and is periodic in x with period ℓ . This periodicity reflects the periodic arrangement of the monomers that form the filament. For example, in the case of myosin motors, the period would be of the order of the actin monomer size if one neglects the chirality of the actin filaments. The particles switch between the two states with an attachment rate $\omega_{\text{on}}(x)$ and a detachment rate $\omega_{\text{off}}(x)$. These transition rates are not specified for the moment, but they are smooth positive functions of x , periodic with period ℓ , and we assume that their inverse are of the order of a characteristic transition time t_m that lies in the range $t_m \sim 10$ ms. We also assume that the detailed balance condition is not satisfied ($\omega_{\text{off}}/\omega_{\text{on}} \neq \exp(W/k_B T)$) in order to reflect the energy consumption coming from the hydrolysis of ATP molecules. We denote by $\omega(x)$ the sum of the attachment and detachment rates: $\omega(x) = \omega_{\text{on}}(x) + \omega_{\text{off}}(x)$. In the limit of a large number of motors ($N \gg 1$), we define the density of attached motors $\rho(x, t)$, which is normalized such that $N\rho(x, t)dx$ is the number of motors in the attached state at time t whose positions are inside any interval of the type $[x + n\ell, x + n\ell + dx]$, with n integer. The function $\rho(x, t)$ is then periodic in x , with period ℓ . We assume that the total number of motors at each position does not depend on x : the density of motors in the detached state is therefore $1/\ell - \rho(x, t)$. This hypothesis is satisfied when the motors are uniformly distributed along the backbone (as in a motility assay experiment) or when they are regularly spaced with a period incommensurate to the filament period (as in muscles). The equation for motor conservation reads then

$$\partial_t \rho - \dot{X} \partial_x \rho = -\omega_{\text{off}}(x)\rho + \omega_{\text{on}}(x)(1/\ell - \rho). \quad (1)$$

The terms on the right-hand side of this equation are due to the transition events, whereas one finds the convective flux of motors on the left-hand side, with \dot{X} the filament instantaneous velocity in the reference frame of the backbone. The position of the filament is $X(t)$. The force F_m exerted by the motors on the filament is given by

$$F_m = N \int_0^\ell \rho(x, t) \partial_x W(x) dx. \quad (2)$$

The evolution of the position X is driven by the force balance equation on the filament

$$\xi \dot{X} = F_{\text{ext}} + F_m. \quad (3)$$

Here, we have assumed the existence of a viscous friction term, with a drag coefficient ξ . This coefficient is at least as high as the hydrodynamic drag, but could possibly be larger in the presence of other sources of dissipation. We do not discuss the physical origin of the friction, but we determine the different accessible regimes when ξ is varied. Whatever its origin, we expect that ξ is proportional to the length of the filament, and therefore to the number of interacting motors. The force balance equation (3) assumes that the friction is equilibrated by the motor force F_m and by an external force F_{ext} . We consider in this paper the two cases of a constant external force and of an elastic force of stiffness k ($F_{\text{ext}} = -kX$). Equations (1) and (3) define $X(t)$ and $\rho(x, t)$ at all times t . We stress that these equations are valid only if the number of motors is large enough so that fluctuations can be neglected. Fluctuations in motor assemblies are theoretically considered in other papers [11, 30, 31]. The natural microscopic length scale of the model is the filament period ℓ , which we chose as our length unit ($\ell = 1$), even if sometimes, we re-establish the homogeneity in some equations by writing ℓ explicitly.

Some calculations can be done in the general case, but we also examine two particular choices for the transition rates: the uniform rate approximation and the localized rate approximation, represented in fig. 1. In the *uniform rate approximation*, we assume that the sum $\omega_{\text{on}}(x) + \omega_{\text{off}}(x) = \omega$ does not depend on x . Calculations using this approximation have been carried out for the first time in ref. [6]. This approximation is convenient when the transition rates are almost uniform. They are periodic functions and can be characterized by their Fourier series: $\omega_{\text{on}}(x) = \sum_{q \geq 0} [\alpha_q \cos(2\pi qx) + \beta_q \sin(2\pi qx)]$. In the case of weakly varying transition rates, the coefficients of the Fourier modes tend rapidly to zero when $q \rightarrow \infty$. The simplest approximation consists in keeping only the first Fourier mode:

$$\omega_{\text{on}}(x) = \omega[\eta - \alpha(\cos(2\pi x) - \varepsilon \sin(2\pi x))], \quad (4)$$

$$\omega_{\text{off}}(x) = \omega[1 - \eta + \alpha(\cos(2\pi x) - \varepsilon \sin(2\pi x))]. \quad (5)$$

Here, η represents the fraction of attached motors (averaged over x) and is sometimes called the “duty ratio”, α is the amplitude of variation of the transition rates and ε is a positive dimensionless parameter. The parameter ω is

the sum of the transition rates, and we identify it with the inverse of the characteristic transition time ($t_m = \omega^{-1}$). The potential $W(x)$ is also described by its first Fourier mode: $W(x) = U[1 - \cos(2\pi x)]$. It is symmetric, but the system does not show the “left-right” symmetry because there is a finite shift between the transition rates and the potential when $\varepsilon \neq 0$. The motors are symmetric when $\varepsilon = 0$.

The second limiting case that we consider is the *localized rate approximation*, where one assumes that the detachment rate is localized on a region of size d at the bottom of the potential: in this region, its value is $\omega_{\text{off}}^{\text{max}}$, whereas it vanishes outside this region (fig. 1(b)). We also assume a uniform attachment rate. Equivalently, we could chose an attachment rate localized at the top of the potential and a uniform detachment rate to reflect the existence of binding sites [32]. The characteristic transition time is identified with the inverse of the attachment rate: $t_m = \omega_{\text{on}}^{-1}$. In fig. 1(b) we have also represented the potential that we choose, which is piecewise linear and asymmetric.

The localized rate approximation can be seen as the opposite of the uniform rate approximation, because all the Fourier modes of the detachment rate are non-zero in the limit $\omega_{\text{off}}^{\text{max}} \rightarrow \infty$, and one cannot restrict the study to the first Fourier modes. Note that in both cases we choose the asymmetry parameters ($\varepsilon > 0$, $a < 1/2$) so that the motors exert a positive force on the filament when this one is at rest. Several authors have used the uniform rate approximation to describe the motion of flagella and cilia [6, 33] or the oscillations of hair bundles in the inner ear [8], whereas other studies assume localized rates [15, 11, 12, 22]. It is therefore interesting to determine up to which point the behaviors of the model in these regimes are generic.

When the filament moves at constant velocity $\dot{X} = v$, the motor force reaches a stationary value $F_m(v)$. We define the *force-velocity relation* as the relation between the velocity v and the external force that has to be applied so that the filament velocity is v . This relation takes into account the viscous force and the motor force: $F_{\text{ext}}(v) = \xi v - F_m(v)$. It is known that the force-velocity curves can be non-monotonic in this model, giving rise to hysteresis effects when the external force is constant [15]. It is also known that, in the presence of a weak external elastic load, oscillations can be obtained in this model [34]. The study of the rigid two-state model that we carry out in the next sections aims at clarifying its general properties and determining which parameters control the oscillation regimes.

2.2 Motor force for a prescribed trajectory of the filament

We start our analysis by deriving a formula which gives the density of motors ρ as a functional of the trajectory $X(t)$. Let us assume that $X(t)$ is known in eq. (1), in which we suppress the convective term by a change of reference frame: we let $y = x + X(t)$ and define $\bar{\rho}(y, t) = \rho(x, t) =$

$\rho(y - X(t), t)$. We obtain

$$\partial_t \bar{\rho} + \omega(y - X(t)) \bar{\rho} = \omega_{\text{on}}(y - X(t)), \quad (6)$$

where, as above, we have written $\omega(x) = \omega_{\text{on}} + \omega_{\text{off}}$. Multiplying by $\exp[\int_{t_0}^t dt' \omega(y - X(t'))]$ (where t_0 is a fixed time), we recognize a first-order derivative on the left hand-side

$$\partial_t \left[\bar{\rho} e^{\int_{t_0}^t dt' \omega(y - X(t'))} \right] = \omega_{\text{on}}(y - X(t)) e^{\int_{t_0}^t dt' \omega(y - X(t'))}. \quad (7)$$

After integration over t , we obtain the following expression at large times for the original variable $\rho(x, t)$:

$$\rho(x, t) = \int_0^\infty d\tau \omega_{\text{on}}(x + X(t) - X(t - \tau)) \times e^{-\int_0^\tau dt' \omega(x + X(t) - X(t - t'))}. \quad (8)$$

Inserting this result into eq. (2) provides a formal expression for the motor force F_m as a functional of the position $X(t)$ of the filament, which gives an exact solution of the model. The motor force depends on the positions of the filament $X(t')$ at all times t' earlier than t . The exponential factor in eq. (8) implies that the motor force only depends on the positions of the filament at times t' such that $t - t'$ is smaller than $[\min \omega(x)]^{-1}$. As the position $X(t')$ appears explicitly in this exponential factor, the associated “memory time” can depend on $X(t)$ itself. In the next sections we give a precise definition of the memory time and use eq. (8) to compute the force-velocity relations in some limiting cases. Note that spatial translational invariance is respected in eq. (8): the density (and therefore the motor force) does not change if one applies a translation $X(t) \rightarrow X(t) + X_0$.

2.3 Force-velocity relation and memory time

2.3.1 Localized detachment rate

Equation (8) can be simplified in the case of localized rates. Let us define $\tau^*(x, t)$ as the time spent since the motors that are now at position x at time t passed in front of a detachment site for the last time. Then, for $x \in [a-1; a]$, the time $\tau^*(x, t)$ is calculated as the minimal value that satisfies one of the two equations:

$$\begin{cases} x + X(t) - X(t - \tau^*(x, t)) = a - 1 + d/2, \\ x + X(t) - X(t - \tau^*(x, t)) = a - d/2. \end{cases} \quad (9)$$

In eq. (8), the contributions coming from $\tau > \tau^*$ give terms that are negligible in the limit $\omega_{\text{off}}^{\text{max}} \rightarrow \infty$. One can then approximate ρ by

$$\rho(x, t) = \int_0^{\tau^*(x, t)} d\tau \omega_{\text{on}} e^{-\omega_{\text{on}} \tau} = 1 - e^{-\omega_{\text{on}} \tau^*(x, t)}. \quad (10)$$

The meaning of this expression is clear: the density at position x increases with the time τ^* spent since the last passage at a detachment site. It vanishes just after this

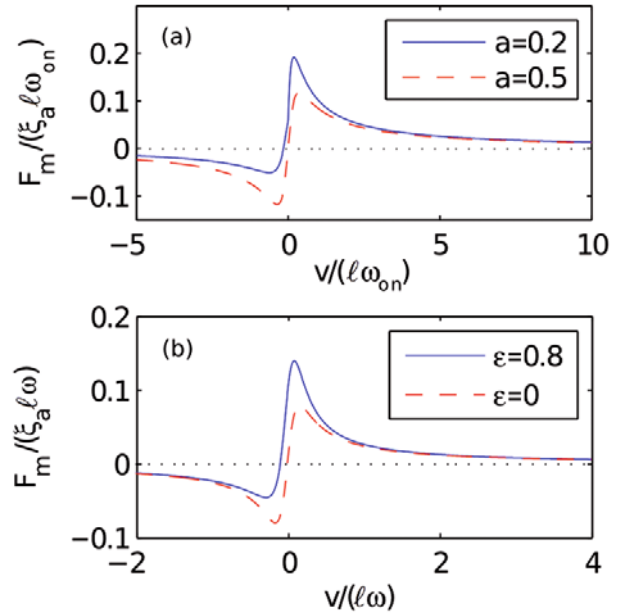


Fig. 2. Typical relations between motor force and filament velocity for the rigid two-state model, obtained in the localized rate approximation (a) (with $\omega_{\text{off}}^{\text{max}} = \infty$, $d = 0.1$) and the uniform rate approximation (b). On each graph, we have represented a curve for symmetric motors ($a = 1/2$, or $\varepsilon = 0$) and a curve for asymmetric motors.

passage (when $\tau^* = 0$): the motors that pass in front of a detachment site detach instantaneously in the limit where $\omega_{\text{off}}^{\text{max}} \rightarrow \infty$. The expression (10) can be used to compute the force-velocity relation. At a constant velocity $\dot{X} = v > 0$, the solution of eq. (9) is $\tau^* = (a - d/2 - x)/v$, which we insert into eqs. (10), (2) to obtain an analytic formula for the force-velocity relation

$$F_m = \frac{NU}{a(1-a)} \left[\frac{d(1-2a)}{2} + \frac{v}{\omega_{\text{on}}} \left(1 - e^{\frac{\omega_{\text{on}}(-a+d/2)}{v}} + a(-1 + e^{\frac{\omega_{\text{on}}(-1+d)}{v}}) \right) \right]. \quad (11)$$

The typical shape of the force-velocity relation is represented in fig. 2(a). The force varies over the characteristic velocity scale $l\omega_{\text{on}}$. Expanding eq. (11) for large v shows that $F_m \sim 1/v$. Under stall conditions (at vanishing velocity $v = 0$), the force is proportional to d : $F_m = F_{\text{stall}} = NUd(1-2a)/(2a(1-a))$. The behavior for negative velocities is obtained by doing the transformation $a \rightarrow 1-a$. At small velocities, the force varies linearly with the velocity, but the analysis is complicated because there is a discontinuity of the slope of the force-velocity relation around $v = 0$; this discontinuity has no physical meaning and comes from the discontinuities of the transition rates. The linear analysis reveals that the important parameter is the mean slope of the force-velocity relation at zero velocity ξ_a , which we call the effective friction coefficient

$$\xi_a = \frac{NU}{2a(1-a)\omega_{\text{on}}}. \quad (12)$$

We also define the *memory time* t_{mem} at velocity v as the time to wait until the force reaches its stationary value. This memory time is smaller than the time to wait before all the motors reach a detachment site ℓ/v , and it is also smaller than the attachment time ω_{on}^{-1} according to eq. (10). Therefore,

$$t_{\text{mem}} \sim \min(\omega_{\text{on}}^{-1}, \ell/v). \quad (13)$$

For symmetric motors ($a = 1/2$), we obtain a much simpler force-velocity relation

$$F_{\text{m}} = \frac{2NUv}{\omega_{\text{on}}} \left(1 - e^{\frac{(-1+d)\omega_{\text{on}}}{2|v|}}\right)^2. \quad (14)$$

2.3.2 Uniform rate approximation: dynamical system

In the uniform rate approximation, we can derive equations for the evolution of the Fourier modes of the density, defined by $\rho(x, t) = \alpha \sum a_q(t) \cos(2\pi qx) + b_q(t) \sin(2\pi qx)$. The various modes are coupled only by the convective term of eq. (1). We find that only the modes (a_1, b_1) play a role, and we denote $a = a_1, b = b_1$. The force is given by $F_{\text{m}} = N\pi U \alpha b$, and the evolution of (a, b) is given by the two-dimensional dynamical system

$$\begin{cases} \dot{a} + \omega a - 2\pi \dot{X} b = -\omega, \\ \dot{b} + \omega b + 2\pi \dot{X} a = \varepsilon \omega. \end{cases} \quad (15)$$

This expression illustrates clearly that the memory time associated to the motors is $t_{\text{mem}} \sim \omega^{-1}$, in agreement with eq. (8) (where the “kernel” is a single exponential $\exp(-\omega\tau)$). The force-velocity relation is easily obtained by looking at the fixed points of the system (15) when $\dot{X} = v = \text{constant}$

$$F_{\text{m}} = \xi_a \left(v + \frac{\varepsilon \ell \omega}{2\pi} \right) \frac{1}{1 + 4\pi^2 (v/(\ell\omega))^2}, \quad (16)$$

where the active friction coefficient ξ_a is

$$\xi_a = \frac{2\pi^2 N \alpha U}{\omega \ell^2}. \quad (17)$$

The force-velocity relation is displayed in fig. 2(b) and is similar to that obtained for localized detachment rate.

2.3.3 Shape of the force-velocity relation in the general case

We now show that the shape of the force-velocity relation is not arbitrary in the rigid two-state model. In the general case, eqs. (8), (3) enable to formally calculate the force-velocity relation. Two limits are of interest. In the limit of small velocities, we have $F_{\text{m}} = F_{\text{stall}} + \xi_a v$, with

$$F_{\text{stall}} = N \int_0^1 dx \frac{(\partial_x W) \omega_{\text{on}}(x)}{\omega_{\text{on}}(x) + \omega_{\text{off}}(x)}, \quad (18)$$

$$\xi_a = N \int_0^1 dx \frac{\partial_x W}{\omega_{\text{on}}(x) + \omega_{\text{off}}(x)} \frac{\partial}{\partial x} \frac{\omega_{\text{on}}(x)}{\omega_{\text{on}}(x) + \omega_{\text{off}}(x)}. \quad (19)$$

The “stall force” F_{stall} is the force exerted by the motors at zero velocity, and ξ_a can be interpreted as the opposite of an effective friction coefficient. It is useful to look at the case where the detailed balance condition is satisfied ($\omega_{\text{off}} = \omega_{\text{on}} e^{W/k_B T}$), where $F_{\text{stall}} = \int dx (\partial_x W) / [1 + \exp(W/k_B T)] = 0$ vanishes, and where ξ_a becomes

$$\xi_a = -N \int_0^1 dx \frac{(\partial_x W)^2 e^{\frac{W}{k_B T}}}{(\omega_{\text{on}} + \omega_{\text{off}}) k_B T \left(1 + e^{\frac{W(x)}{k_B T}}\right)^2} < 0. \quad (20)$$

Hence, if the detailed balance condition is satisfied, the coefficient ξ_a is negative: the transition events give rise to a large passive friction. The coefficient ξ_a can be positive only if the detailed balance condition is not satisfied, leading to a motor behavior.

The second interesting limit is that of large velocities. In this case (see appendix A.1), we find that the force varies as $1/v$, with a coefficient

$$F_{\text{m}} \simeq -\frac{N}{\bar{\omega} v} \int_0^1 dx \int_0^1 dy \int_0^y dz [\partial_x W(x)] \omega_{\text{on}}(x+y) \omega(x+z), \quad (21)$$

where we have defined the mean value of the sum of the transition rates $\bar{\omega} = \int_0^1 \omega(x) dx$. The force always tends to zero for large velocities $v \gg \ell/t_{\text{m}}$, and the force-velocity relation has a hyperbolic shape for large velocities. This is to be compared to the hyperbolic force-velocity relation measured in muscles as given for example by Hill’s relation. The fact that the motor force $F_{\text{m}} \sim 1/v$ is an intrinsic property of the rigid two-state model and is due to the periodicity of the transition rates and of the potential. This calculation shows that the force-velocity relation is not arbitrary in the rigid two-state model: the motor force remains finite only in a range of velocities ℓ/t_{m} , and tends to zero for larger velocities.

2.3.4 Stability of the force-velocity relation

We discuss the stability of the force-velocity relation. Let us assume a constant external force F_{ext} . The system reaches a stationary state with constant velocity v_S that lies on the force-velocity relation and therefore satisfies the equation $F_{\text{ext}} = \xi v_S - F_{\text{m}}(v_S)$. This equation can have several solutions if the force-velocity relation is non-monotonic. It would be tempting to guess that a solution located in a region where the slope of the force-velocity relation $(\partial_v F_{\text{ext}})$ is positive (respectively negative) corresponds to a stable solution (respectively unstable). This statement would be true if the force depended on the instantaneous velocity. However, this statement is not correct as the force at time t depends on the velocity at all earlier times $t' < t$. We illustrate this fact in the case of the uniform rate approximation for symmetric motors ($\varepsilon = 0$). In this case, the evolution of the system is given by the two-dimensional dynamical system (15) with $\dot{X} = v_S$. The evolution of the deviations of the variables with respect to their stationary state ($\delta a = a - a_S$ and $\delta b = b - b_S$) is given by a linear differential equation

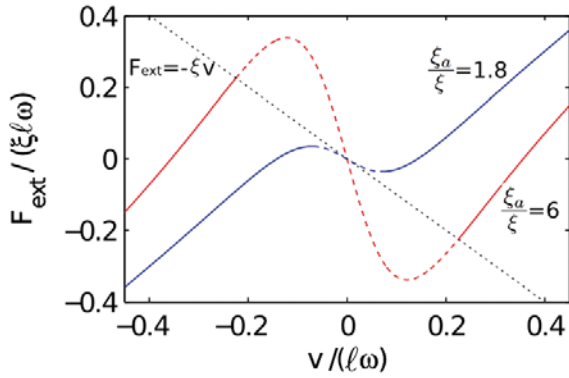


Fig. 3. Force-velocity relations ($F_{\text{ext}}(v) = \xi v - F_m(v)$) in the uniform rate approximation for two values of ξ_a/ξ represented together with the line of equation $F_{\text{ext}} = -\xi v$. The dashed parts of the curves are unstable in conditions of constant external forces, while the full-line parts are stable. Note that for $\xi_a/\xi = 6$, some regions of the force-velocity relation with positive slope are unstable.

$(\partial_t \delta a, \partial_t \delta b) = -M(\delta a, \delta b)$, where M is a 2 by 2 matrix (see appendix A.2 for calculation details). The determinant of M is proportional to $\partial_v F_{\text{ext}}$, which proves that a solution located on a region of the force-velocity relation with negative slope is always unstable. The reciprocal is not true because the trace of M is given by

$$\text{Tr}(M) = (\omega/v_S)(v_S + F_{\text{ext}}/\xi). \quad (22)$$

The trace of M vanishes on the line $(\xi v_S + F_{\text{ext}}) = 0$ in the force-velocity plane. It turns out that for $\xi_a/\xi > 8/3$, a part of the branch with positive slope corresponds to unstable steady-state solutions (fig. 3). Therefore, the stability of the force-velocity relation cannot be deduced only from its shape, even if it is true that all regions with negative slope are necessarily unstable. This conclusion has to be compared with the results of stochastic simulations performed in ref. [30] where it is observed that some branches of the force-velocity relation that are apparently stable are never reached by the system.

2.4 Dynamics in the presence of an elastic force: oscillations

We now focus on the case where the motor assembly is submitted to an external elastic force with stiffness k which vanishes at position $X = 0$: $F_{\text{ext}} = -kX$. The only existing stationary state is the one with zero velocity where the elastic force compensates the motor stall force. As the motor force amounts to a negative friction at small velocities, this state can be unstable. In the model of rigid motors, the force due to the motors remains finite (because the maximal force per motor is bounded by $\sim U/\ell$), so that the filament cannot go infinitely far from the position $X = 0$. Numerical integration shows that the trajectory of the filament is periodic with time: oscillations appear, in

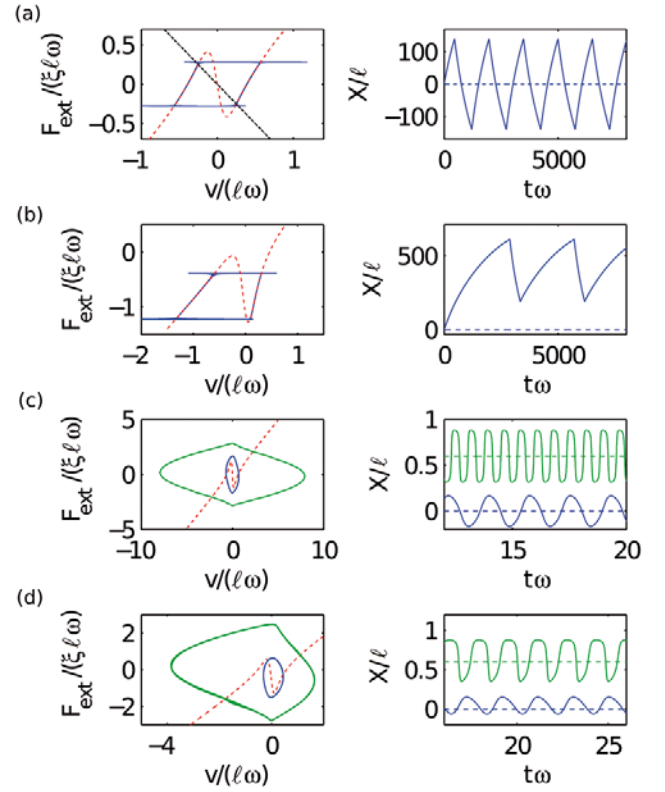


Fig. 4. Examples of oscillations in the rigid two-state model, with the uniform rate approximation. On the graphs on the left, trajectories (continuous lines) are plotted in the force-velocity plane ($\dot{X}, F_{\text{ext}} = -kX$) together with the stationary force-velocity relation (dashed lines). On the graphs on the right, the same trajectories are plotted in the plane $(t, X(t))$ (continuous curves) together with the position of the center of the elastic external force (dashed horizontal lines). The oscillations on the graphs (a) and (b) are relaxation oscillations. On each of the graphs (c) and (d), we show both rectangular and weakly non-linear oscillations. The motors are symmetric in (a) and (c) and asymmetric in (b) and (d). Parameter values: (a): $k/(\xi\omega) = 0.002$, $\xi_a/\xi = 7$, $\varepsilon = 0$. (b): same as (a) except for $\varepsilon = 1$. (c): $k/(\xi\omega) = 10$, $\varepsilon = 0$, $\xi_a/\xi = 17$ (small-amplitude oscillation) and $\xi_a/\xi = 300$ (larger-amplitude oscillation). (d): $k/(\xi\omega) = 10$, $\varepsilon = 0.3$, $\xi_a/\xi = 13$ (small-amplitude oscillation) and $\xi_a/\xi = 50$ (larger-amplitude oscillation).

agreement with the predictions of ref. [12]. In fig. 4, several types of oscillations are represented: we distinguish the weakly non-linear oscillations (with a shape close to a sinusoid, in the vicinity of the bifurcation threshold) from non-linear oscillations, which can be of “cusplike” shape (with large amplitude and period) or “rectangular” (with amplitude and period comparable to the microscopic length and time scale). We now give a detailed analysis of the various oscillation regimes in the case of the uniform rate approximation for symmetric motors, and then we highlight the differences that can appear for other choices of transition rates.

2.4.1 Hopf bifurcation and memory effect

In the case of the uniform rate approximation, the evolution of the system is described by a 3-dimensional dynamical system (see eq. (15)):

$$\begin{cases} \dot{a} + \omega a - 2\pi \dot{X} b = -\omega, \\ \dot{b} + \omega b + 2\pi \dot{X} a = \varepsilon \omega, \\ \xi \dot{X} = -kX + F_m = -kX + \xi_a \omega b / (2\pi). \end{cases} \quad (23)$$

The only fixed point of this system is ($a = -1$, $b = \varepsilon$, $X = X_s = \xi_a \omega \varepsilon / (2\pi k)$). We expand around the fixed point ($\delta a = a + 1$, $\delta b = b$, $\delta X = X - X_s$). We omit the equation for δa which decouples from the two others and we use the variable $\delta f = \xi_a \omega \delta b / (2\pi)$ instead of δb . δf represents the motor force increment with respect to the stall force. We obtain

$$\delta \dot{f} + \omega \delta f = \xi_a \omega \delta \dot{X}, \quad (24)$$

$$\xi \delta \dot{X} = -k \delta X + \delta f. \quad (25)$$

Equation (24) shows that the motor force δf amounts to a delayed negative friction (of coefficient ξ_a), with a delay $t_m = \omega^{-1}$: the force is therefore not proportional to the instantaneous velocity. If we eliminate the variable δf , we obtain a second-order equation for X

$$\frac{\xi}{\omega} \delta \ddot{X} + \left(\xi - \xi_a + \frac{k}{\omega} \right) \delta \dot{X} + k \delta X = 0. \quad (26)$$

This equation contains an effective mass $m = \xi/\omega$, which comes from the interaction between the delay ω^{-1} in the motor force and the friction ξ . Equation (26) predicts an oscillatory instability if

$$\xi_a - \xi > k\omega^{-1} (= kt_m). \quad (27)$$

Expression (27) implies that a motor assembly can be stable even if the force-velocity relation has a negative slope near the origin: the stiffness k stabilizes the system. This can be understood from the following argument. Let us assume that, at $t < 0$, the system is in its stationary state, and that a fluctuation brings it to a state with small positive velocity v for $t > 0$. This fluctuation is amplified if the elastic stabilizing force is smaller than the motor destabilizing force. The elastic force varies as $kX = kv t$, whereas the motor force behaves at short times as $\xi_a v (t/t_m)$ due to the delay t_m (fig. 5). The elastic force therefore stabilizes the system if $k > \xi_a/t_m$, which agrees with the threshold condition (27) in the limit $\xi \rightarrow 0$. The stabilization by the external stiffness is therefore due to a *memory effect*. Equation (27) that gives the oscillation threshold is very general, and it can be written as

$$\text{Effective friction} > (\text{Stiffness}) \times (\text{Memory time}). \quad (28)$$

We checked that this formula is also valid in the case of localized transition rates up to a numerical factor (see appendix A.3 for details). A similar memory effect is present in models that describe stick-slip oscillations in tribology [35–37]. In fact, other analogies exist with models of

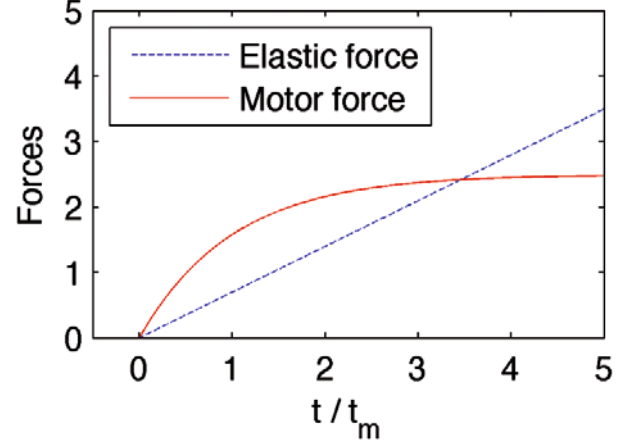


Fig. 5. Schematic representation of the elastic force $kv t$ (in absolute value) and the motor force $F_m = \xi_a v [1 - \exp(-t/t_m)]$ in response to a velocity step $X = vtH(t)$.

stick-slip, for which one can also define a non-monotonic force-velocity relation and observe relaxation oscillations that look like relaxation oscillations of motor assemblies. For this reason, oscillations of motor assemblies could be seen as a sort of spontaneous stick-slip oscillations.

In the case of the uniform rate approximation, we used standard techniques of non-linear physics to identify the resonant terms and to show that the Hopf bifurcation is super-critical: close to the threshold, the amplitude of the weakly non-linear oscillations is given by

$$A = \frac{2\ell}{\pi} \sqrt{\frac{(\xi_a - \xi - kt_m)(\xi + 4kt_m)}{3kt_m(2kt_m + \xi)}}. \quad (29)$$

The oscillations with this small amplitude have almost a sinusoidal shape (see an example in fig. 4(c)). Note that there is no reason why the bifurcation be super-critical in the general case. In fact, we found that it can be sub-critical if one includes second harmonics for the potential and the transition rates. From eq. (26), we see that the frequency of these weakly non-linear oscillations is, at lowest order in the distance to the threshold

$$f_c = \frac{1}{2\pi} \sqrt{\frac{k\omega}{\xi}}. \quad (30)$$

This frequency is the geometric mean of the inverse of the two characteristic times of the system: the passive relaxation time in the harmonic potential (ξ/k) and the delay in the motor force $t_m = \omega^{-1}$. This results holds up to a numerical factor in the case of localized transition rates as well (see appendix A.3). Equation (30) implies that the frequency of oscillations can be arbitrarily higher than the inverse of the chemical time t_m if the stiffness is high, and if $(\xi_a - \xi) \sim kt_m$ (in order to remain in the regime of weakly non-linear oscillations). This result implies that oscillations due to motor assemblies could describe the mechanisms of high-frequency oscillations, such as insect wingbeat, as originally noted in ref. [15].

2.4.2 Amplitude and period of relaxation oscillations

We now focus on the “cusplike” oscillations (represented in fig. 4(a)). We call them “relaxation oscillations” because they are characterized by the presence of two different timescales: they appear when the time to reach the force-velocity relation is small compared to the period of the oscillations. The system evolves along the stable branches of the force-velocity relation. This suggests an adiabatic approximation: we assume that the force F_m depends on the instantaneous velocity, and that the system switches to the other branch of the force-velocity relation as soon as it reaches an unstable region. The amplitude A is estimated by noting that the force at which the branch of the force-velocity relation becomes unstable is $kA/2$. As we have seen in section 2.3.4, the force-velocity relation becomes unstable when $\partial_v F_{\text{ext}} = 0$ if $\xi_a/\xi < 8/3$ and when $F_{\text{ext}} = -\xi v$ if $\xi_a/\xi > 8/3$. We pose $\gamma = \xi_a/\xi$, $r(\gamma) = \gamma(\gamma+8)$ and find the following expression for the amplitude A :

$$A = \frac{\ell\xi\omega}{k} \times \begin{cases} \frac{(3\gamma-\sqrt{r})[\sqrt{r}-2-\gamma]^{\frac{1}{2}}}{\sqrt{2\pi}(-\gamma+\sqrt{r})}, & \text{if } \gamma < \frac{8}{3}, \\ \sqrt{\frac{\gamma-2}{2\pi^2}}, & \text{if } \gamma > \frac{8}{3}. \end{cases} \quad (31)$$

The period is estimated by considering the evolution of X in the adiabatic approximation, which satisfies the equation

$$\xi\dot{X} - F_m(\dot{X}) = -kX. \quad (32)$$

This equation can be integrated between $t = 0$ (where $X = -A/2$) and $t = T/2$ (where $X = A/2$) by a method of separation of variables. We express the result as

$$T = \frac{\xi}{k} \tilde{h}(\gamma), \quad (33)$$

where $\tilde{h}(\gamma)$ is a dimensionless function of $\gamma = \xi_a/\xi$ that can be determined numerically and is given in fig. 6. We obtain the asymptotic value of $\tilde{h}(\gamma)$ by noting that, for large values of γ , only branches where $v \sim \sqrt{\gamma}$ are visited, which enables to approximate the force by its limit for large velocities: $F_m \sim \xi_a\omega^2/(4\pi^2v)$ and we explicitly integrate eq. (32) to obtain

$$T = \left(\frac{3}{2} + 2\ln 2\right) \frac{\xi}{k} \simeq 2.886 \frac{\xi}{k}. \quad (34)$$

This expression is confirmed by numerical integration (fig. 6). The system is in this regime when the memory time ω^{-1} is smaller than the characteristic time of the evolution of X , which can be identified with the period $T \sim \xi/k$. The adiabatic approximation is therefore valid when $k \ll \xi\omega$. An important result is that both the period and the amplitude vary as the inverse of the stiffness k in the limit of small stiffnesses, and can therefore be arbitrarily high compared to the microscopic length and time scale when $k \rightarrow 0$. The large and slow relaxation oscillations are the result of the collective behavior of the motors and do not depend much on the microscopic details. In the case where $\varepsilon > 0$, oscillations are no longer

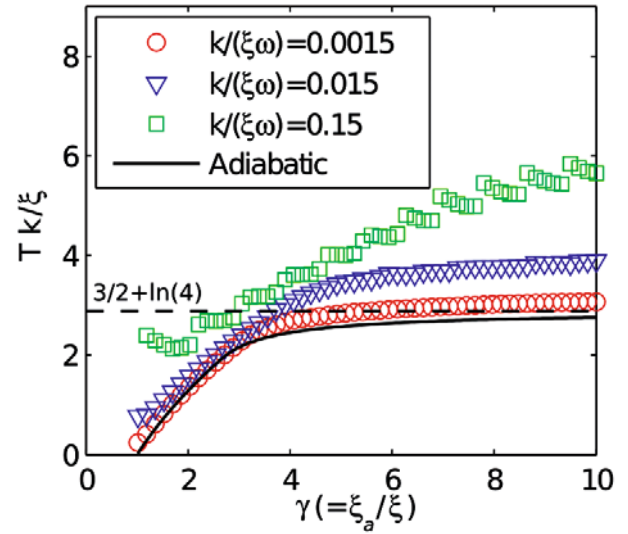


Fig. 6. Normalized period of relaxation oscillations for the uniform rate approximation. Symbols are the result of numerical integration of the dynamical system (23), the continuous line represents the theoretical result of the adiabatic approximation in the limit $k \rightarrow 0$ (function \tilde{h} in eq. (33)). The dashed horizontal line is the value of \tilde{h} for $\gamma \rightarrow \infty$ (eq. (34)).

symmetrical (fig. 4(b)): the phase in the positive direction is slower than the phase in the negative direction. This behavior is very robust in the general case and is in agreement, for example, with the properties of oscillations in myofibrils, where the contraction phase is much slower than the elongation phase [38].

2.4.3 Small rectangular oscillations

For large values of k , we find oscillations with “rectangular” shape (if the motors are symmetric, $\varepsilon = 0$, see example in fig. 4(c)). Their period is of the order of ω^{-1} and the amplitude is quantized and equal to a multiple of half the period of the potential, $A \sim n\ell/2$, with n an integer. These oscillations are made of rapid phases (where X varies by $\sim \ell/2$) followed by slower phases (that last $\sim \omega^{-1}$, where X remains almost constant). The projection of the trajectory in the force-velocity plane is very far from the steady-state force-velocity relation (fig. 4(c) and (d), left). This is not surprising, since in this regime, the time ξ/k of evolution along the force-velocity relation is smaller than the memory time ω^{-1} , so that the motor force does not depend only on the instantaneous velocity. The fact that the amplitude is close to $\ell/2$ can be understood from the following argument. We assume that $X(t) = -A/2 + AH(t)$, where H is the Heaviside step function, and A is the amplitude of the oscillations, which is also the amplitude of the jump in the rapid phase. Then, substituting the rates given by eqs. (4) and (5) into eq. (8) and integrating over x , we find that the force after the jump is

$$F_m = \frac{\xi_a\omega}{2\pi} \sin(2\pi A)e^{-\omega t}. \quad (35)$$

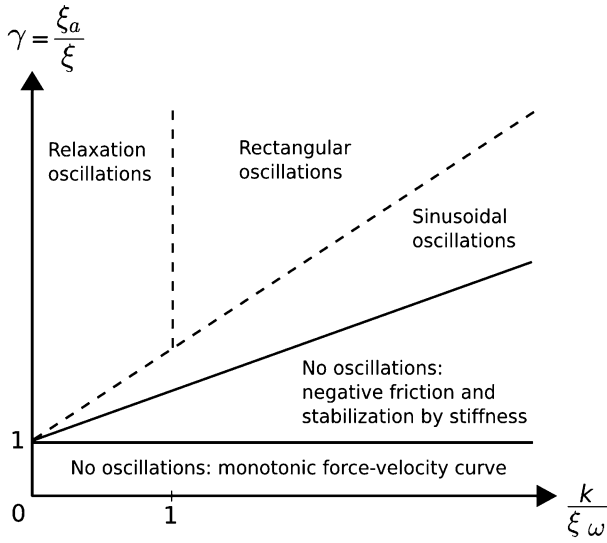


Fig. 7. Schematic diagram showing the different oscillation regimes that are accessible in the uniform rate approximation for the rigid two-state model. The dashed lines are only qualitative.

At short times, this force derives from the effective potential, $V_{\text{eff}}(A) = \xi_a \omega \cos(2\pi A)/(4\pi^2)$, whose minima are at positions $-1/2, 1/2, 3/2, \dots$. The position $A = 0$ is therefore unstable: the filament rapidly moves until it reaches a stable position in a minimum of V_{eff} at $A = \pm \ell/2$. This reasoning is valid if the elastic force is negligible, *i.e.* when $\xi_a \gg k/\omega$. Equation (35) shows that the motor force vanishes with time, which explains why the filament slowly comes back to the position $X = 0$ with a time scale ω^{-1} . The filament position becomes unstable when the stiffness of the effective potential is smaller than k , in which case another jump occurs. These oscillations occur in the limit of large stiffness, or small friction, and should be compared to other oscillations obtained in a regime of small friction in another model [39], in which the oscillation amplitude is also of molecular size.

2.4.4 Summary: oscillation regimes

The various types of oscillations that appear in the uniform rate approximation for the rigid two-state model are summarized on the diagram presented in fig. 7. Right above the Hopf bifurcation threshold, one finds weakly non-linear oscillations. If one increases the parameter $\gamma = \xi_a/\xi$, one obtains relaxation oscillations for low values of the stiffness, and rectangular oscillations for high values of k . The only regime in which the frequency can be much higher than t_m^{-1} is the regime of weakly non-linear oscillations, the model predicts that the amplitude of these fast oscillations is smaller than the microscopic length scale ℓ . Observations of asynchronous flight muscles seem to indicate that the strain is 1–3% [40], implying sliding displacements between actin and myosin of 11–33 nm, which are possibly larger than $\ell \sim 5$ nm, which seems to be in contradiction with our prediction. However, fast

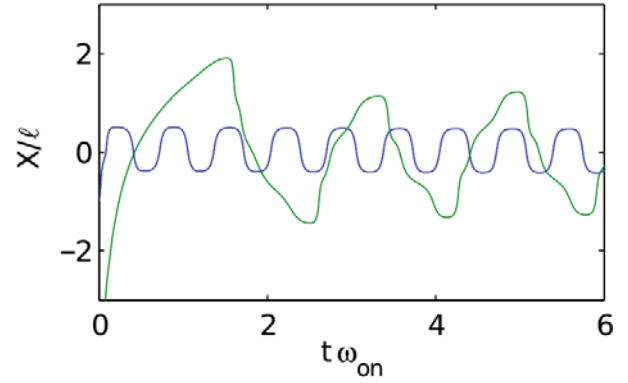


Fig. 8. Oscillations for localized rate, with $a = 1/2$, $d = 0.1$, $\omega_{\text{off}}^{\text{max}} = 200$, $k/(\xi\omega_{\text{on}}) = 5$, and $\xi_a/\xi = 100$. Note that the curves have identical parameters, only the initial conditions are different.

oscillations with larger amplitudes could possibly appear with other hypotheses than the uniform rate approximation. The very quick oscillations of insect flight muscle could also come from an accelerated chemical cycle, as suggested in ref. [41].

2.4.5 Co-existing limit cycles for the localized rate approximation

In the case of the localized rate approximation, we observed the same types of oscillations as in the uniform rate approximation. A memory effect also exists, and the position of the threshold is therefore given by a formula similar to eq. (27) (appendix A.3). A difference with the uniform rate approximation is the amplitude of the small rectangular oscillations, which is close to ℓ instead of $\ell/2$. The reason is that the force after a jump of size A is given by an analogous of formula (35)

$$F_m = e^{-\omega_{\text{on}} t} [W(\ell/2 - A) - W(\ell/2)] N/\ell^2. \quad (36)$$

This force vanishes at $A = \ell$, which explains the amplitude of the rectangular oscillations.

Another difference is that relaxation oscillations can be obtained for larger values of k in the localized rate approximation than with the uniform rate approximation. The reason is that the memory time scales as $1/v$ for large velocities instead of remaining of the order of t_m (eq. (13)), and relaxation oscillations that explore branches of force-velocity relations with large velocities are therefore possible. We checked that relaxation oscillations can appear for any value of the stiffness, provided that the value of the effective friction ξ_a is high enough. Contrary to the uniform rate approximation, the oscillation period in this regime is not limited by $T \sim \xi/k$, as we observed oscillations with a period $T \sim 15\xi/k$.

A last difference with the uniform rate approximation is the co-existence of several limit cycles for specific values of the parameters; the limit cycle chosen by the system then depends on the initial conditions (fig. 8). This additional source of hysteresis in motor assemblies could have

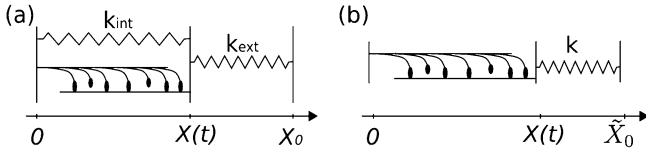


Fig. 9. (a) Motor assembly connected to external and internal elastic elements. (b) Equivalent system with no internal elastic element.

important consequences. For example, in an experiment where the noise is weak, it could be possible to observe several oscillation cycles with two different frequencies and amplitudes with the same system. Experiments on muscles mention the fact that, sometimes, relaxation oscillations disappear and appear therefore only as a metastable state [42]. This could be understood if the limit cycle with large amplitude is less stable than the limit cycle with small amplitude. It could also be understood if the Hopf bifurcation is subcritical. Molecular motor assemblies could thus be an example of system that displays two distinct frequencies without requiring the presence of two distinct oscillators.

2.5 Force-displacement relation

Force-displacement relations are commonly measured on muscular systems [43], or on hair-bundles of the vertebrate inner ear [44]. We now investigate what is the typical shape of the force-displacement relation for the rigid two-state model. Due to the memory effect, the oscillations can always be suppressed if the motor assembly is connected to a high enough external stiffness. Here we consider a slightly more general case in which the motor assembly is connected to an internal elastic element of stiffness k_{int} , and is submitted to an external elastic force $F_{\text{ext}} = -k_{\text{ext}}(X - X_0)$ centered around the position X_0 (fig. 9(a)). The internal stiffness would represent for example the passive stiffness of a sarcomere or a hair-bundle. We further assume that no oscillations occur ($\xi_a - \xi < (k_{\text{int}} + k_{\text{ext}})t_m$). The system can be probed by applying a perturbation and by then observing the relaxation dynamics to the stationary state. We consider here a perturbation where X_0 is changed by a quantity Δ at time $t = 0$. The relation between the force $F_{\text{ext}}(\Delta, t_{\text{exp}})$ at a time t_{exp} and the displacement Δ for various values of Δ is called the “force-displacement relation at time t_{exp} ”. We first note that the system is equivalent to a system with no internal elastic element (represented in fig. 9(b)), with an equivalent stiffness $k = k_{\text{int}} + k_{\text{ext}}$, for which one would replace X_0 (and Δ) by an equivalent displacement $\tilde{X}_0 = X_0 k_{\text{ext}}/k$ (and $\tilde{\Delta} = \Delta k_{\text{ext}}/k$) and add a linear elastic component $k_{\text{int}}\tilde{\Delta}$ to the external force. For this reason, the case $k_{\text{int}} = 0$ can be considered without loss of generality. We assume in the following that $k_{\text{int}} = 0$, and keep the notations $k = k_{\text{ext}}$, $\tilde{\Delta} = \Delta$. Note also that “displacement clamp conditions” (or “isometric conditions”) are also available in our analysis by taking the limiting case $k = \infty$. Typical experimental curves in muscular systems

or in the hair bundle of the inner ear show non-linear zones [43, 44], which are usually interpreted in terms of the molecular details of the system components. Here, we show that the rigid two-state model naturally generates non-linear force-displacement relations, suggesting that these non-linearities could be seen as the signature of the vicinity of a dynamic instability.

Translational invariance implies that the force F_m tends to the stall force F_{stall} when $t \rightarrow \infty$, so that the force-displacement curve at large times is simply the horizontal line $F_{\text{ext}} = -F_{\text{stall}}$. Two limiting cases have to be discussed. The first limiting case is that of infinitely high stiffness ($k \gg \xi/t_m$). This case is very close to the case where the displacement $X(t)$ is controlled by an external feedback system. The motors have little influence on the dynamics of X , and it is possible to analytically compute the force by inserting the *ansatz* $X(t) = \Delta H(t)$ into eq. (8). We find that the density ρ is given by

$$\rho(x, t) = \rho_{\text{stat}}(x) + H(t)[\rho_{\text{stat}}(x + \Delta) - \rho_{\text{stat}}(x)]e^{-\omega(x)t}, \quad (37)$$

where we define the density in the stationary state $\rho_{\text{stat}}(x) = \omega_{\text{on}}/\omega$. This formula is valid for any choice of transition rates. The important remark is that this expression is periodic in the variable Δ , and so are the force-displacement relations. In fact, this result is not surprising: if the motors do not have the time to attach or detach when the filament is displaced, the situation after and before the displacement step is not different if this displacement is equal to an integer number of periods. Such periodic behavior of the force-displacement relation however has never been measured to our knowledge.

The second limiting case is the case of weak stiffness, for which the system has time to follow the force-velocity relation: the behavior then depends only on the shape of the force-velocity relation, and not on the details of the model. Let us consider the case of asymmetric motors, close to the value at which the system oscillates. The response is plotted in fig. 10 and is very asymmetric. A perturbation in the positive direction has only a small effect on the response, whereas a displacement in the negative direction eventually brings the system to another branch of the force-velocity relation and has a very strong effect on the response. In this case, the force does not relax monotonously to its stationary value, but shows an “overshoot”. This behavior qualitatively resembles the twitch observed in the hair-bundle [45] or the “give” of a sarcomere observed in response to an elongation [46]. This behavior is characteristic of the response of an *excitable medium* [47].

This non-linear response implies the existence of non-linearities in force-displacement relations, as can be seen in fig. 10. The non-linearity is more pronounced on the side of negative direction. The size of the non-linear zone can be large compared to the period ℓ : because the characteristic time and length-scales are $\sim 1/k$ (cf. eq. (32)), if the stiffness is divided by a factor p , then the size of the non-linear zone is multiplied by this factor p if the

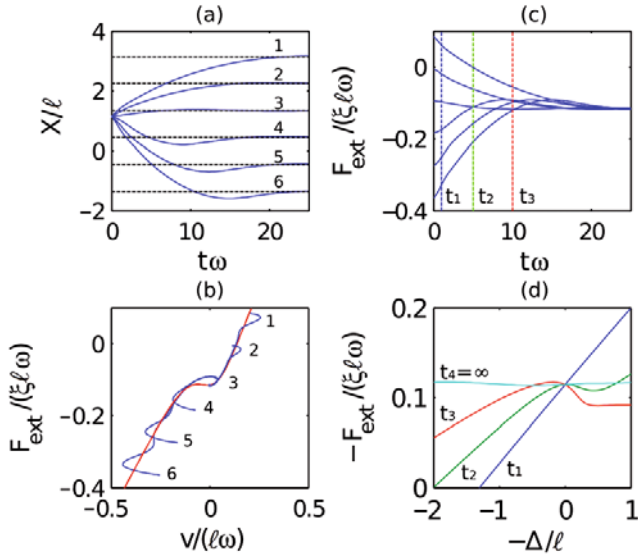


Fig. 10. Response to a displacement step for the rigid two-state model in the uniform rate approximation in the limit of weak stiffness. (a) Filament position $X(t)$ (continuous lines) in response to displacements steps of the external force of Δ (indicated by the dotted lines). (b) Same curves represented in the force-velocity plane. (c) Relaxation curve of the force $F_{\text{ext}} = -k(X - \Delta)$ for the same values of Δ . (d) Resulting force-displacement relation at 4 different times $t_1 = 1$, $t_2 = 5$, $t_3 = 10$, $t_4 = \infty$ in units of ω^{-1} . We represent the curves $(-F_{\text{ext}}, -\Delta)$ instead of (F_{ext}, Δ) in order to have the same sign convention as tension *vs.* length step curves in muscles. Parameters: $\gamma = 0.9$; $\varepsilon = 0.8$; $k/(\xi\omega) = 0.1$.

measurement time is also multiplied by p . On the contrary, we note in fig. 10 that the non-linearity is already present at short times ($t_{\text{exp}} = 5\omega^{-1}$) and that the size of the non-linearity is comparable to the filament period. The force-displacement curve for positive displacement steps looks very much like the original tension-length measurement of Huxley and Simmons [43]. Note also that our relations present a well-pronounced negative slope, whereas in muscles the curves are rather “flat”. However, a recent study has shown that this difference can come from inhomogeneities present in a group of sarcomeres [48]. It was already known that force-displacement relations with negative slope could emerge in a particular 3-state crossbridge model that displayed an instability. Our results show that this holds true for the rigid two-state model as well, suggesting that non-linear force-displacement relations exist for systems in the vicinity of a dynamic instability.

3 Instabilities in crossbridge (power-stroke) models

In the second part of this paper, we study the properties of a crossbridge (or “power-stroke”) model, focussing on the similarities and the differences with the rigid two-state model.

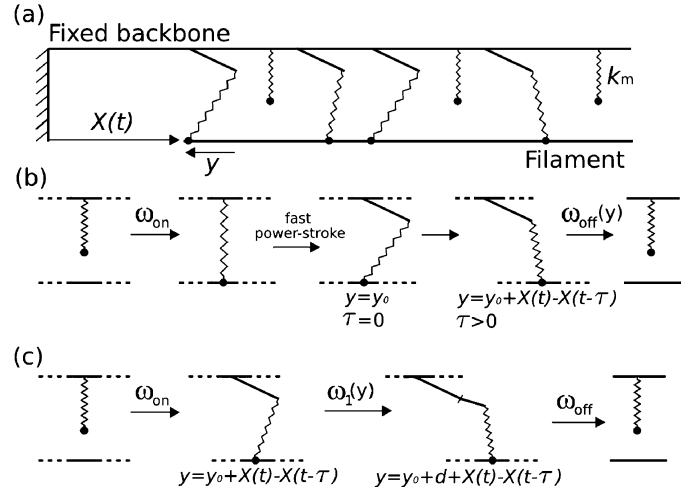


Fig. 11. (a) Sketch of a motor assembly in the crossbridge model. (b) Hypotheses for the individual motor behaviour in the two-state crossbridge model with continuous binding sites. (c) Hypotheses for the 3-state crossbridge model (see text, sect. 3.6.1).

3.1 Equations for the crossbridge model

The two-state crossbridge model is sketched in fig. 11(a),(b). We consider N motors tightly bound on a fixed backbone, that can interact with a filament at position $X(t)$. The motors are represented by springs of finite stiffness k_m . We assume that a detached motor can bind in front of its linking point to the backbone anywhere on the filament and that it binds with zero strain. We call ω_{on} the attachment rate. A more general model would include discrete attachment sites periodically spaced on the filament with a period b . In the limit where only one site is accessible for each motor ($b \rightarrow \infty$), one obtains the original Huxley crossbridge model [28]. We study here the opposite limit (first introduced in ref. [49]) where the binding sites are continuously distributed ($b \rightarrow 0$). Just after the attachment, a conformational change, in general called the power-stroke brings the motors in a “pre-stressed” state where the elongation is y_0 . We assume that $y_0 < 0$, so that a motor that just got attached exerts a positive force ($-k_m y_0$) on the filament. The head of a motor remains stuck on the filament until detachment. We call τ the time elapsed since a motor attached, the strain at time t is $y = y_0 + X(t) - X(t - \tau)$. The variable τ can also be called the “age of contact”. The motors detach with a strain-dependent detachment rate $\omega_{\text{off}}(y)$. This assumption is motivated by experiments on myosin molecules showing that the lifetime of the attached state is load-dependent [50,51]. In the limit of a large number of motors, we describe the motor assembly by a density $\rho(\tau, t)$, which we normalize so that the number of motors at t that attached between the times $t - \tau$ and $t - \tau + \Delta t$ is $N\rho\Delta t$. The equation for the conservation of the motor number reads

$$\partial_t \rho + \partial_\tau \rho + \omega_{\text{off}}(y_0 + X(t) - X(t - \tau))\rho = \omega_{\text{on}}\delta(\tau)(1 - n), \quad (38)$$

where $n(t)$ is the fraction of bound motors at t

$$n(t) = \int_0^\infty d\tau \rho(\tau, t). \quad (39)$$

The force exerted by the motors on the filament is

$$F_m = -N \int_0^\infty d\tau \rho(\tau, t) k_m (y_0 + X(t) - X(t - \tau)). \quad (40)$$

We again assume that the filament motion results from the force balance involving a frictional term, an external force and the motor force

$$\xi \dot{X} = F_{\text{ext}} + F_m. \quad (41)$$

The attachment term proportional to $\delta(\tau)$ of equation (38) can be considered as a boundary condition for $\tau = 0$ by looking for solutions of the type $\rho = H(\tau)\tilde{\rho}$. We obtain: $\tilde{\rho}(0, t) = \omega_{\text{on}}(1 - n(t))$. Note that we chose to use the variable τ instead of the variable y , but that the equations with the variable y are completely equivalent (see appendix A.4).

3.2 Force-velocity relation

We begin the analysis of the crossbridge model by rederiving the force-velocity relation (already calculated in refs. [49, 14]). Solving eq. (38) with $\dot{X}(t) = v = \text{constant}$ and inserting into eq. (40) gives

$$F_m = \frac{-\omega_{\text{on}} k_m N \int_0^\infty d\tau (y_0 + v\tau) e^{-\int_0^\tau d\tau' \omega_{\text{off}}(y_0 + v\tau')}}{\omega_{\text{on}} \int_0^\infty d\tau e^{-\int_0^\tau d\tau' \omega_{\text{off}}(y_0 + v\tau')} + 1}. \quad (42)$$

This expression formally defines the relation $F_m(v)$ for any choice of function ω_{off} . At small velocities, we obtain $F_m = F_{\text{stall}} + \xi_a v$, with

$$F_{\text{stall}} = N k_m |y_0| \frac{\omega_{\text{on}}}{\omega_{\text{on}} + \omega_{\text{off}}(y_0)}, \quad (43)$$

$$\xi_a = \frac{N k_m \omega_{\text{on}}}{[\omega_{\text{off}}(y_0) + \omega_{\text{on}}] \omega_{\text{off}}(y_0)} \left[-1 + \frac{-\omega'_{\text{off}}(y_0) |y_0|}{\omega_{\text{on}} + \omega_{\text{off}}(y_0)} \right]. \quad (44)$$

The stall force and the effective friction thus depend only on the properties of the detachment rate function ω_{off} in the vicinity of the point y_0 . Expression (44) has been obtained in ref. [14]. The meaning of the expression of the stall force F_{stall} is clear: at vanishing velocity, the motors attach with elongation y_0 and detach with the same elongation. The fraction of bound motors is $\eta = \omega_{\text{on}}/[\omega_{\text{on}} + \omega_{\text{off}}(y_0)]$, and the force is therefore $N\eta|y_0|k_m$. The effective friction ξ_a (eq. (44)) always contains a negative (passive) term $-N\eta k_m/\omega_{\text{off}}$, which can be identified as a protein friction [52] and which is analogous to friction in rubber materials [53]: this friction is due to the energy dissipated by the elongated springs when the motors detach. There is a second contribution to ξ_a which appears only if the detachment rate is not uniform, and

which makes the total friction negative if the following condition is satisfied:

$$\xi_a > 0 \Leftrightarrow \omega'_{\text{off}}(y_0) y_0 > \omega_{\text{on}} + \omega_{\text{off}}(y_0). \quad (45)$$

A necessary condition to obtain a negative friction ($\xi_a > 0$) is $\omega'_{\text{off}}(y_0) y_0 > 0$: the detachment rate must increase with the absolute value of the elongation. In other words, the detachment rate must increase when the motor head is submitted to an increasing load.

3.3 Oscillations

In crossbridge models, the effective friction can be negative ($\xi_a > 0$), implying that oscillatory solutions exist in the presence of an elastic external force. The linear analysis is described in appendix A.5. We find that there is a Hopf bifurcation when

$$\begin{cases} \xi_a > \xi + k t_m + 0(k^2), & \text{if } k \rightarrow 0, \\ \xi_a > k \left(\frac{1}{\omega_0} + \frac{1}{\omega_0 + \omega_{\text{on}}} \right), & \text{if } k \rightarrow \infty, \end{cases} \quad (46)$$

where $\omega_0 = \omega_{\text{off}}(y_0)$ and t_m is a complicated function of k_m and ξ/N , that always remains of the order of the inverse of the transition rates ($t_m \sim \omega_0^{-1} + (\omega_0 + \omega_{\text{on}})^{-1}$ when $\xi/N \rightarrow 0$, and $t_m \sim \omega_0^{-1} + \omega_0(\omega_0 + \omega_{\text{on}})^{-1}(2\omega_0 + \omega_{\text{on}})^{-1}$ when $k_m \rightarrow 0$). The instability condition (46) is very similar to the instability condition (28) of rigid motors. They have the same physical origin: the stiffness of the external spring stabilizes the system due to a memory effect. We also calculate the frequency at the oscillatory instability threshold:

$$f_c = \frac{1}{2\pi} \sqrt{\frac{k\omega_0(\omega_0 + \omega_{\text{on}})}{k + \eta k_m N + \xi(2\omega_0 + \omega_{\text{on}})}}. \quad (47)$$

As in the case of rigid motors (eq. (30)), the frequency grows as \sqrt{k} for small k . A difference with the case of rigid motors is that the frequency remains smaller than $[\omega_0(\omega_{\text{on}} + \omega_0)]^{1/2}/(2\pi) \sim t_m^{-1}$ even if $k \rightarrow \infty$ or $\xi \rightarrow 0$. Unlike in the case of rigid motors, it is not possible to obtain frequencies significantly higher than the inverse of the motor characteristic transition time t_m (except if one of the times of the cycle step is small). This might be due to the existence of the protein friction that naturally appears in this model. Assuming that k and ξ are weak, we can write $f_c \sim \sqrt{k}/(\xi_{\text{protein}} t_m)$, where $\xi_{\text{protein}} = N\eta k_m/\omega_0$ is the protein friction. This expression is similar to the corresponding formula for rigid motors (eq. (30)). The occurrence of protein friction enables to obtain weakly non-linear oscillations much slower than in the case of rigid motors.

Although we did not carry out a detailed analysis of the oscillation regimes as in the case of rigid motors, we observed the presence of weakly non-linear oscillations as well as relaxation oscillations represented in fig. 12. As in the case of (asymmetric) rigid motors, these oscillations

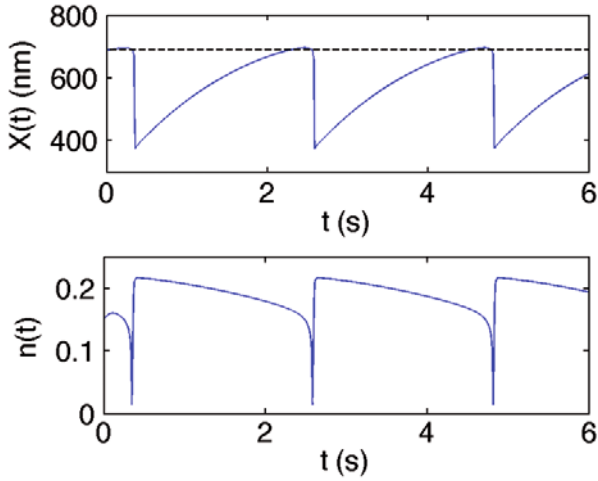


Fig. 12. Example of oscillations obtained with the crossbridge model, far from the instability threshold. Top: filament position $X(t)$ (continuous line) and unstable stationary position (dashed line). Bottom: fraction of bound motors $n(t)$. Parameters: $k = 0.1$ pN/nm, $N = 40$, $\omega_{\text{off}} = \bar{\omega}_0(1 + y^2/2/a^2)$, with $a = 3$ nm, $\bar{\omega}_0^{-1} = 20$ ms, $\xi = 0.6$ pN ms/nm, $k_m = 2$ pN/nm, $\omega_{\text{on}}^{-1} = 40$ ms, power-stroke size: $y_0 = -5.7$ nm.

show a slow phase in the direction of the motors spontaneous motion and a fast phase in the other direction. The mechanism of these oscillations is directly linked to the load dependence of detachment rate: close to the stall conditions, any reduction in the number of attached motors will increase the tension on the remaining motors and trigger their faster detachment. The fast phase of the oscillations is therefore associated to the detachment of all the motors at the same time, as can be seen in fig. 12.

3.4 Force-displacement relation

We now look at the response to a displacement step of the origin of the elastic force in order to determine the force-displacement relation for the crossbridge model. As in the case of the rigid model, we have to distinguish the limits of small and high external stiffness. In the limit of small stiffness k , the response essentially depends on the shape of the force-velocity relation, and the system response is again similar to that of an excitable medium. Force-displacement relations in this case display large non-linear zones whose sizes are not limited by molecular details.

In the limit of large external stiffness ($k \gg Nk_m + \xi t_m$), we can assume that the displacement is imposed: $X(t) = \Delta H(t)$, where $H(t)$ is the Heaviside function. Contrarily to the rigid two-state model, the force-displacement relation in this regime does not show spatial periodicity, and can be analytically calculated by noting that, when $t > 0$, two populations of motors exist. The motors that were initially attached and that are still attached at time t have elongation $y_0 + \Delta$. Their fraction is $n_1 = \int_t^\infty d\tau \rho(\tau, t)$ and they detach with detachment rate $\omega_{\text{off}}(y_0 + \Delta)$. The second population contains the motors that attached after

the initial time and have an elongation y_0 ; their fraction is $n_0 = \int_0^t d\tau \rho(\tau, t)$. These motors detach with the detachment rate $\omega_{\text{off}}(y_0)$. Then, by integrating eq. (38) over τ , we find that n_0 and n_1 satisfy the equations

$$\dot{n}_0 = \omega_{\text{on}} - (\omega_0 + \omega_{\text{on}})n_0 - \omega_{\text{on}}n_1, \quad (48)$$

$$\dot{n}_1 = -\omega_1 n_1, \quad (49)$$

where we have set $\omega_0 = \omega_{\text{off}}(y_0)$ and $\omega_1 = \omega_{\text{off}}(y_0 + \Delta)$. We define the fraction of bound motors at stall conditions $\eta = \omega_{\text{on}}/(\omega_{\text{on}} + \omega_0)$, and we integrate eqs. (48), (49) with the initial conditions $n_1(0) = \eta$, $n_0(0) = 0$, leading to the following expression for the force:

$$\begin{aligned} F_m - F_{\text{stall}} &= -Nk_m[n_1(y_0 + \Delta) + n_0 y_0] \\ &= Nk_m \eta \left[-\Delta e^{-\omega_1 t} \right. \\ &\quad \left. + \frac{|y_0|(\omega_1 - \omega_0)}{\omega_0 - \omega_1 + \omega_{\text{on}}} \left(e^{-(\omega_0 + \omega_{\text{on}})t} - e^{-\omega_1 t} \right) \right]. \end{aligned} \quad (50)$$

Several remarks can be done. At short times, $F_m - F_{\text{stall}} \sim -Nk_m \eta \Delta$: the force comes from the finite elasticity of the motors. We can also calculate the slope of the force-displacement relation at time t for small displacements ($k_{\text{eff}}(t) = -(\partial_\Delta F_m)_{\Delta=0}$):

$$k_{\text{eff}}(t) = Nk_m \eta \omega_{\text{on}}^{-1} e^{-\omega_0 t} [(\omega_{\text{on}} - \alpha y_0) + \alpha y_0 e^{-\omega_{\text{on}} t}], \quad (51)$$

where we noted $\alpha = \omega'_{\text{off}}(y_0)$. This equation defines an apparent stiffness, which is negative for at least one time if the following condition is satisfied:

$$\exists t / k_{\text{eff}}(t) < 0 \Leftrightarrow \omega'_{\text{off}}(y_0) y_0 > \omega_{\text{on}}. \quad (52)$$

This condition is less restrictive than the condition to obtain a positive ξ_a (which requires $\omega'_{\text{off}}(y_0) y_0 > \omega_{\text{on}}/\eta$). Hence, it is possible to observe non-linear force-displacement relations without observing oscillations if the elastic force is lowered, but the presence of oscillations necessarily implies the existence of a region with negative slope in the force-displacement relation. In fig. 13, we have represented the force-displacement relation in the limit of high external stiffness of the system that generates the oscillations of fig. 12. We clearly distinguish a region with an apparent negative stiffness, and the curve looks like the experimental measurements on shortening muscles of refs. [43, 54]. Note, however, that the precise shape of the curve depends on the choice of the detachment rate function, which we have chosen arbitrarily. These results indicate that the observation of non-linear force-displacement relations is not incompatible with the presence of oscillations if the external stiffness is lowered, and is an intrinsic property of crossbridge models, even with only two states.

3.5 Delayed stretch activation

The ‘‘delayed stretch activation’’ is the response of a muscle after a small stretch, characterized by an initial rise of

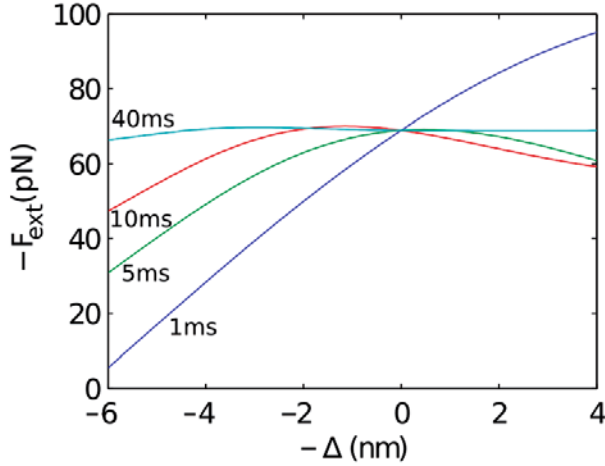


Fig. 13. Force-displacement curves at several times for the crossbridge model with the parameters that generated the oscillations shown in fig. 12, except for $k = \infty$ (displacement clamp conditions). We inverted the signs so that the curve has the same sign conventions as in muscle measurements (tension *vs.* length step curves).

the tension followed by a decay, and then at larger times by an another rise in tension that is interpreted as the delayed activation of crossbridges under stretch. This response is characteristic of insect flight muscles and cardiac muscles [55]. We discuss this concept here and make a link with the “delayed negative friction” response that appears in both rigid and crossbridge models. We come back to the rigid two-state model in the uniform rate approximation, where, for small displacements $\delta X(t)$, the motor force is given by $F_m = F_{\text{stall}} + f$ (see eq. (24)), with

$$f(t) = \int_{-\infty}^t dt' \omega \xi_a \delta \dot{X}(t') e^{-(t-t')\omega}. \quad (53)$$

This equation expresses the fact that the force is a delayed negative friction. After integrating by parts, we find

$$f(t) = \omega \xi_a \delta X(t) - \omega^2 \int_{-\infty}^t dt' \xi_a \delta X(t') e^{-(t-t')\omega}. \quad (54)$$

One can then interpret the force as the sum of an instantaneous negative stiffness, and a delayed positive elastic force. The second component of the force can be identified with a delayed increase in tension. If δX is a step displacement, $\delta \dot{X} = \Delta H(t)$, the measured force increase is $F_{\text{ext}} = \xi \dot{X} - f + k_{\text{int}} \Delta$ (where we include a term for the internal elasticity)

$$F_{\text{ext}} = \xi \Delta \delta(t) - \xi_a \omega \Delta + \xi_a \omega \Delta (1 - e^{-\omega t}) + k_{\text{int}} \Delta. \quad (55)$$

This force is represented in fig. 14(a). There is a first initial phase which is due to the friction (viscous peak), followed by a rapid decay (due to the effective negative elasticity $-\xi_a \omega$) and at larger times an apparent delayed increase in tension (term proportional to $(1 - e^{-\omega t})$). For the crossbridge model, we obtain a similar curve, the tension is now deduced from eq. (51) and is represented in fig. 14(b).

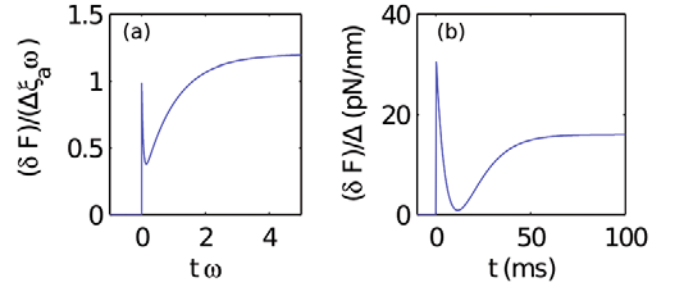


Fig. 14. Qualitative force response to a displacement step of small amplitude $X(t) = \Delta H(t)$ for the rigid two-state model (a) and the crossbridge model (b). For the rigid two-state model we have added an arbitrary viscous peak and assume that $k_{\text{int}} = 1.2 \xi_a \omega$. For the crossbridge model, we assume that the parameters are such that $\omega_{\text{on}}^{-1} = 40$ ms, $\omega_{\text{off}}^{-1}(y_0) = 10$ ms, $k_m = 2$ pN/nm, $y_0 = -10$ nm, $k_{\text{int}} = 16$ pN/nm, $N = 40$, $\omega'_{\text{off}}(y_0) y_0 = 4 \omega_{\text{off}}(y_0)$.

The main difference is then the short time response, which is due to the motor elasticity in the crossbridge model rather than a viscous peak. These curves are very similar to the experimental delayed stretch activation curves of refs. [56,57]. We stress, however, that the final value of the tension has been introduced somehow artificially in our model: we either assume an internal elasticity, or that motors are recruited when the muscle is stretched. Other hypotheses (reviewed in [17]) could also be proposed to explain the stretch activation. Importantly, we note that the fact that the minimum of the tension curve is close to zero means that the internal elasticity k_{int} is of the order of ξ_a/t_m , or, in other words, that the system is close to the instability threshold and could generate weakly non-linear oscillations, which could be fast in the case of the rigid two-state model. It has already been suggested that the crossbridge model could generate an apparent delayed stretch activation [58,59] with numerical simulations. Here, we have shown that this result also holds for the rigid two-state model, because the delayed negative friction naturally generates an apparent delayed stretch activation.

3.6 Link with single-molecule experiments

We now discuss the link between single-molecule experiments and the collective behavior of molecular motors. An experiment on the myosin subfragment S1 [60] suggests that this type of myosins detaches faster when submitted to an opposing force, as required to obtain an instability. The measurements indicate an exponential detachment rate $\omega_{\text{off}} \sim \exp(-k_m y a / k_B T)$, with $a = 1$ nm, and $k_m = 1.8$ pN/nm. This experiment can be interpreted with the two-state crossbridge model. Assuming a power-stroke size of $y_0 = -5$ nm, we find that $|\omega'_{\text{off}}(y_0) y_0| / \omega_{\text{off}}(y_0) = k_m a |y_0| / k_B T \simeq 2 > 1$. These motors could therefore generate dynamic instabilities. Other single-molecule experiments on myosin show an apparent load-decelerated dissociation rate [51,61], indicating that these motors could

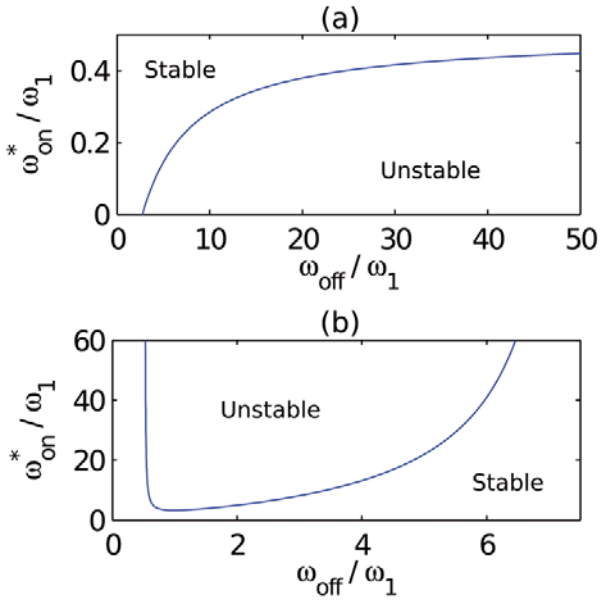


Fig. 15. Stability diagrams for the 3-state crossbridge model. $|y_0| = |d|$. (a): $\omega'_1/\omega_1 = -1.5$ (load-accelerated dissociation rate), (b): $\omega'_1/\omega_1 = 10$ (load-decelerated dissociation rate). The lines separate the unstable regions from the stable regions. Units of length are chosen such that $|d| = 1$.

not generate instabilities when they are in groups. However, the interpretation of these experiments is difficult within the framework of a two-state model because of the existence of 3 states. In the next section, we determine the instability condition for a 3-state crossbridge model.

3.6.1 Instability condition in a 3-state model

The 3-state crossbridge model that we consider is represented in fig. 11(c). It is the same model as the 2-state crossbridge model, but we now assume that the motors can switch to a second attached state at a rate $\omega_1(y)$. During this transition, the motors undergo a second conformational change of size $d < 0$. Then the motors detach with a rate that we assume uniform for simplicity. An expression for the effective friction ξ_a is calculated in appendix A.6, and we find that the critical value of ω_{on} for which ξ_a vanishes is given by

$$\frac{\omega_{on}^*}{\omega_1} = -\frac{\frac{\omega_{off}}{\omega_1} \left(1 + \frac{\omega_{off}}{\omega_1} + \frac{\omega_{off}^2}{\omega_1^2} \right) - \frac{\omega'_1(y_0)y_0}{\omega_1} \frac{\omega_{off}^3}{\omega_1^3}}{1 + 2\frac{\omega_{off}}{\omega_1} + \left(2 + \frac{\omega'_1(y_0)d}{\omega_1} \right) \frac{\omega_{off}^2}{\omega_1^2} + \frac{\omega_{off}^3}{\omega_1^3}}, \quad (56)$$

where we have introduced $\omega_1 = \omega_1(y_0)$. This expression is a rational fraction of the variable ω_{off}/ω_1 and has a meaning only if $\omega_{on}^* > 0$. It defines a line of instability in a plane $(\omega_{off}/\omega_1, \omega_{on}/\omega_1)$ for fixed values of y_0 , d , $\omega'_1(y_0)/\omega_1$ (fig. 15). The analysis of eq. (56) indicates that an instability can occur in the case of an apparent load-accelerated detachment rate if $\omega'_1(y_0)y_0/\omega_1(y_0) > 1$. In this case, the instability occurs for large detachment rates

and low attachment rates (fig. 15(a)). If $\omega'_1(y_0) > 0$, an instability occurs for intermediate values of the detachment rate and large values of the attachment rate, but only if the value of the second power-stroke is large enough ($|\omega'_1(y_0)d/\omega_1(y_0)| > 5.219$) (fig. 15(b)).

It is therefore possible to obtain an instability in both cases of an apparent load-accelerated dissociation rate ($\omega'_1(y_0) < 0$) and a load-decelerated dissociation rate ($\omega'_1(y_0) > 0$). The instability in the load-accelerated case has the same origin as the instability of the crossbridge model. In the load-decelerated case, the instability comes from the fact that under a positive velocity, a larger population of motors is allowed to do the second power-stroke, and therefore to generate a force that helps the motion. An interesting prediction is that in this case, the instability occurs only in a finite range of detachment rates ω_{off} (and therefore only for a finite range of ATP concentration if ω_{off} is proportional to the ATP concentration [51]). One could imagine that a precise measure of the dependence of the transition rates with the various chemical concentrations could lead to the prediction of instability diagrams of motor assemblies.

In the case of the myosins studied in ref. [51], the parameters are $y_0 = -4$ nm, $d = -2$ nm, $\omega_1(y) = k_0 \exp(k_m y a / k_B T)$, with $a = 2.7$ nm, $k_m = 0.7$ pN/nm and $k_0 = 32$ s⁻¹, so that $|\omega'_1(y_0)d/\omega_1(y_0)| = 0.95 < 5.219$. This estimation suggests that these motors do not generate instabilities when they are in group. Note, however, that the result could be modified by taking into account the discrete nature of the binding sites.

3.6.2 Force-velocity relation and distributions of detachment times in single-molecule experiments

We now give an interpretation of the force-velocity relation (42) in terms of the average time a motor remains attached to the filament and the average force that it exerts while it is attached. These quantities can be measured in single-molecule experiments where a motor interacts with a single filament whose velocity is imposed by holding the two ends of the filament with optical tweezers [60]. We call $Q_v(\tau)$ the distribution of detachment times at a given velocity v . At velocity v , a motor detaches with an effective rate $\omega_{off}(y_0 + v\tau)$ that depends on the time elapsed since the attachment; this rate is related to Q_v through the equation

$$Q_v(\tau) = \omega_{off}(y_0 + v\tau) e^{-\int_0^\tau d\tau' \omega_{off}(y_0 + v\tau')}. \quad (57)$$

We recognize the probability Q_v in the expression of the force-velocity relation eq. (42) by integrating by parts, and identify the moments of the distribution Q_v . If we note $\langle g \rangle_v = \int_0^\infty d\tau g(\tau) Q_v(\tau)$ the average value of any function $g(\tau)$ over the distribution $Q_v(\tau)$, we can write eq. (42) as

$$F_m = -k_m N \frac{\omega_{on}}{\omega_{on} + (\langle \tau \rangle_v)^{-1}} \left(y_0 + v \frac{\langle \tau^2 \rangle_v}{2 \langle \tau \rangle_v} \right). \quad (58)$$

The force is therefore the product of the stiffness of all the motors Nk_m , of the average fraction of time that a motor

spends in the attached state ($\omega_{\text{on}}/(\omega_{\text{on}} + (\langle\tau\rangle_v)^{-1})$) and of a term that measures the variation of the elongation with the velocity (but which is not exactly the average elongation $\langle y_0 + v\tau \rangle_v$). This calculation shows that the force at a given velocity of a motor assembly could be calculated from the measure of the first moments of the distribution of the detachments time in a single-molecule experiment.

4 Discussion

In this paper, we have studied in detail the two kinetic theories that describe the behavior of motor assemblies, the rigid two-state model and the crossbridge model, and we have compared their prediction for various experimental situations. Many of these predictions are similar. The two models generate instabilities linked to the fact that the motor activity creates a force which amounts to a negative friction at low velocities. In both cases, the oscillations are obtained in the presence of an elastic external force and the instability threshold is given by $\xi_a > \xi + kt_m$, where t_m is the characteristic transition time of the motors, which is also the delay of the negative friction force. This oscillation threshold is associated to a memory effect that is also found in several models of stick-slip oscillations [36]. The geometry, the permanent energy dissipation and the shape of the relaxation oscillations are other common points between molecular motor assemblies and stick-slip oscillations. The hypothesis of “shear-induced fluidization” [35], which is sometimes invoked to explain stick-slip oscillations, is very similar to the “load-dependent detachment rate” in crossbridge models. Following the analogy, the slow phase of the asymmetric relaxation oscillations due to molecular motors could be identified with a “stick” phase, whereas the fast phase could be called a “slip” phase. Other analogies with tribology (the science of friction) already exist in the literature: the concept of protein friction [52] is similar to rubber friction [53] and crossbridge models of molecular motors can be adapted to describe friction problems [62]. Recently, the friction force due to molecular motors in the absence of energy consumption [63] has also been measured. Finally, the crossbridge and the rigid two-state models appear as two limiting cases of a more general theory which can be seen as a two-state version of a classical model of solid friction [29].

The two models generate various types of oscillations, including relaxation oscillations with amplitudes and periods that are large compared to the microscopic time and length scales and that are comparable to cardiac sarcomere oscillations. The oscillations appear at a Hopf bifurcation that can be super-critical in both models, leading to weakly non-linear oscillations. Remarkably, the frequency of these oscillations can be arbitrarily high for the rigid two-state model, but not for the crossbridge model. This difference between the two theories is important if one wants to describe the high-frequency oscillations of insect flight muscles, for example. The difference between the two models is related to the role of the passive external friction ξ , which is far less important in the crossbridge

model than in the rigid two-state model, possibly because the crossbridge model naturally generates a friction akin to protein friction. This might be the reason why most studies that use the rigid two-state model must assume high values of the passive friction coefficient ξ [6, 11, 22, 33]. We expect that a large passive friction coefficient would not be necessary to describe the experimental data with the crossbridge model.

The kinetic theories can also account for force-velocity and force-displacement relations. In both models, the variation of the motor force with velocity for large velocities is convex and it is mathematically similar to the Hill relation between tension and contraction velocity for muscles. In the case of the rigid two-state model, we have shown that the force generically decays to zero as $1/v$ for velocities larger than ℓ/t_m . The two kinetic theories also naturally generate non-linearities in the force-displacement relation. If the motor assembly is submitted to a weak elastic load, it behaves as an excitable medium. For large values of the elastic constant k , the force-displacement relations are periodic with the displacement in the case of the rigid two-state model, whereas they show non-linearities in the crossbridge model. Note that a periodic modulation of the force-displacement relation could appear in crossbridge model if the periodicity of the binding sites is considered. These results suggest that non-linearities in the force-displacement relations are not necessarily linked to microscopic details of the molecules but can also emerge in the vicinity of a dynamic instability. We also mention that the response to a small displacement step looks like an *apparent* delayed rise in tension if one introduces artificially an internal stiffness connected to the motor assembly. This apparent “delayed stretch activation” is directly linked to the fact that the motor force amounts at linear order to a delayed negative friction.

Our work also provides new insights on the stability and the hysteresis of molecular motor assemblies. Interestingly, due to the fact that the force is not proportional to the instantaneous velocity, it is *not* possible to deduce the stability of the force-velocity relation only by considering its shape: branches of the force-velocity relation that have positive slope can occasionally be unstable. A similar effect could explain the deviations noted between the results of Monte Carlo simulations and the continuous theory in ref. [30], where these deviations are attributed to a failure of continuous theories. We also showed the possible existence of additional sources of hysteresis in motor assemblies, as several limit cycles can coexist, and the bifurcation can be subcritical. We did not discuss here another possible source of hysteresis particular to the crossbridge model, if the detachment rate vanishes quickly for large strains: in this case, the force given by eq. (42) can diverge to infinity at a given velocity, leading to apparent elastic forces. All of these hysteresis properties of molecular motors could be important with respect to some recently discovered properties of muscles, such as the “residual force enhancement” [64].

Our analytical work should help to discriminate kinetic theories and to provide consistency tests for these

theories. In that respect, analytic formulas for the force-velocity and force-displacement relations, or for the oscillations period and amplitude, could help the comparison between single-molecule experiments data and experiments on motor assemblies, such as sarcomeres or the hair bundles in the inner ear. Furthermore, we found that the parameters of the crossbridge model can be linked to the results of single-molecule experiments: the force-velocity relation can be directly inferred from the measurement of the first moments of the distribution of detachment times in single-molecule experiments (eq. (58)), and one should be able to predict the possible existence of dynamic instabilities for motor assemblies by measuring the detachment rate function in single-molecule experiments. In this respect, we have shown that if one includes a third state, the motor assembly can be unstable even with an apparent load-decelerated detachment rate. Our analytical work could help to test the consistency of the two theories, and eventually discriminate between them. However, their similar properties could make this discrimination difficult. The main difference between the two theories is the role played by friction in the oscillation frequency at threshold, and the qualitative force-displacement relation in isometric conditions. Another way to discriminate between the two theories would be to consider a more general model, the soft-motor model, which contains both kinetic theories as two different limiting cases [29]. Precise measurements of the motor stiffness [60] and potential curvature could enable to estimate the pinning parameter which controls the regimes of the more general theory, and to decide which of the two theories is the most adapted.

Comparison with previous theoretical works. - Finally, we compare our results with previous theoretical studies. We used a crossbridge model with continuous binding sites: this model is a limiting case of the more general crossbridge model studied in ref. [14], and our expression for the effective friction coefficient agrees with the results presented in this reference. We did not consider the opposite limit of discrete binding sites, but we expect that similar instabilities occur in the case of load-dependent detachment rates. An additional phenomenon would be a discontinuity of the slope of the force-velocity relation around the state of zero velocity, as predicted by the soft limit of our “soft-motor model” [29]. Another model has been widely used in the literature [16,23,65,19] and assumes that the motors are active particles described by an individual force-velocity relation that can switch between an unbound and a bound state. In this case also, instabilities are predicted for load-dependent detachment rates, which is similar to the instability of the crossbridge model. A notable difference with the crossbridge model is that one can assume that all the motors have the same strain [16,65]: this approximation becomes exact in the limiting case where the motors relax very fast compared to the detachment time. Such approximations do not correspond to a limiting case of the crossbridge model where the motors are stuck to their filament in the bound state, and one has to consider the strain distribution $p(y, t)$. Self-consistent mean-field approximations have however been

proposed for the crossbridge model to simplify the expressions of the force-velocity relations [30]. Our results could help testing the validity of such approximations. Remarkably, it was observed in ref. [30] that some branches of the force-velocity relation that are apparently stable reveal unstable in stochastic simulations. This result is in good qualitative agreement with our theory (see fig. 3). We generalized the results of [59,13] concerning delayed stretch activation, and the results of [48] concerning the negative slope of the force-displacement relations. The oscillations that we describe are similar to the ones that appear in the literature: one often observes relaxation oscillations [12,23,13]; our work shows that these oscillations occur in the limit of weak external stiffness. The molecular-size oscillations observed in the crossbridge-type model of ref. [39] could be compared to the small rectangular oscillations that occur in the low friction limit of the rigid two-state model.

In conclusion, our detailed study of the rigid two-state model and of the crossbridge model shows that these theories share many similar properties. Both models generate large relaxation oscillations, which look like cardiac oscillations. The rigid two-state model though can generate high-frequency oscillations with a small amplitude unlike the crossbridge model. Experiments based on the response to a step-like displacement of the motor assemblies are also qualitatively well described by both models and nonlinear force-displacement relations, delayed rise in tension, “twitch” and “sarcomere give” qualitatively appear as different limiting cases of kinetic theories. On the experimental side, it seems that a precise independent determination of the parameters of the models is now possible and could allow for a check of the consistency of the two theories. The comparison between single-motor experiments and experiments on motor assemblies would, for example, allow for tests of eq. (58) which would be a strong consistency test of the crossbridge model. Such characterizations could be important to better understand the dynamical behavior of muscles, hair bundles in the inner ear, or flagellar beating.

We thank P. Martin for very stimulating discussions and for drawing our attention on the instabilities that take place in the 3-state crossbridge model. We are also grateful to P.-Y. Plaçais and M. Balland for sharing with us their experimental results.

Appendix A. Calculation details

Appendix A.1. Force at large velocities in the rigid two-state model

Here, we explain how to calculate the large velocity limit of the motor force in the case of the rigid two-state model. We note $\bar{\omega} = \int_0^1 \omega(x) dx$. The mean value of the sum of the attachment and detachment rates is $\bar{\omega} = \int_0^1 \omega(x) dx$, and we define $\delta\omega = \omega - \bar{\omega}$, which is a periodic function of x with

zero average. Its primitive $\delta\Omega = \int \delta\omega$ is also a periodic function. By eq. (6), the density ρ can be written as

$$\rho(x) = \int_0^\infty d\tau \omega_{\text{on}}(x + v\tau) e^{-\frac{\delta\Omega(x+v\tau) - \delta\Omega(x)}{v}} e^{-\bar{\omega}\tau}. \quad (\text{A.1})$$

We decompose the integral in pieces of size $1/v$ (using the formula $\int_0^\infty d\tau = \sum_{n=0}^\infty \int_{n/v}^{(n+1)/v} d\tau$), and for each piece we perform the change in variables $\tau \rightarrow \tau - n/v$. Using the fact that $\delta\Omega$ and ω_{on} are periodic, we obtain

$$\rho(x) = \left(\sum_{n=0}^\infty e^{-\frac{n\bar{\omega}}{v}} \right) \times \int_0^{\frac{1}{v}} d\tau \omega_{\text{on}}(x + v\tau) e^{-\frac{\delta\Omega(x+v\tau) - \delta\Omega(x)}{v}} e^{-\bar{\omega}\tau}. \quad (\text{A.2})$$

The summation over n is simply carried out by recognizing a geometrical series. We change again variables ($X = v\tau$) and we expand at order $1/v$

$$\rho(x) = \left(\frac{v}{\bar{\omega}} + \frac{1}{2} \right) \int_0^1 dX \frac{\omega_{\text{on}}(x + X)}{v} \times \left(1 - \frac{\delta\Omega(x + X) - \delta\Omega(x) + \bar{\omega}X}{v} \right). \quad (\text{A.3})$$

Multiplying by $W'(x)$ and integrating over x gives the result of eq. (21).

Appendix A.2. Stability of the force-velocity relation

We determine here the stability of the force-velocity relation of the rigid two-state model in the case of the uniform rate approximation in the symmetric case ($\varepsilon = 0$). We rewrite here the equations of evolution of the system (see eq. (15))

$$\begin{cases} \dot{a} + \omega a - 2\pi b v = -\omega, \\ \dot{b} + \omega b + 2\pi a v = 0, \end{cases} \quad (\text{A.4})$$

where the velocity v satisfies the equation

$$\xi v = F_{\text{ext}} + F_m = F_{\text{ext}} + \xi_a \omega b / (2\pi). \quad (\text{A.5})$$

Each value of $v = v_S$ corresponds to a unique stationary state (with $a = a_S = -1/(1 + 4\pi^2(v_S/\omega)^2)$ and $b = b_S = -2\pi a_S v_S / \omega$) which defines the force-velocity relation $F_{\text{ext}} = \xi v_S - \xi_a \omega b_S / (2\pi)$. Linearizing around the fixed point, we obtain

$$\frac{d}{dt} \begin{pmatrix} \delta a \\ \delta b \end{pmatrix} = -M \begin{pmatrix} \delta a \\ \delta b \end{pmatrix}, \quad (\text{A.6})$$

where the matrix M is given by

$$M = \begin{pmatrix} \omega & -2\omega\gamma b_S - 2\pi F_{\text{ext}} \\ \omega\gamma b_S + 2\pi F_{\text{ext}} & \omega(1 + \gamma a_S) \end{pmatrix}, \quad (\text{A.7})$$

where $\gamma = \xi_a / \xi$. Substituting a_S and b_S by their values, we calculate the determinant of M and introduce the derivative of F_{ext}

$$\det(M) = \frac{(\omega^2 + 4\pi^2 v_S^2)}{\xi} \left(\frac{\partial F_{\text{ext}}(v)}{\partial v} \right)_{v=v_S}. \quad (\text{A.8})$$

If the determinant is negative, then the matrix M has two eigenvalues of opposite signs and the system is therefore unstable. Equation (A.8) implies that the branches of the force-velocity relation with negative slope are unstable. The reciprocal is not true. The trace of M is given by

$$\text{Tr}(M) = \omega(2 + \gamma a_S) = \frac{\omega(v_S + \tilde{F}_{\text{ext}})}{v_S}, \quad (\text{A.9})$$

where $\tilde{F}_{\text{ext}} = F_{\text{ext}}/\xi$. It vanishes for $(v_S + \tilde{F}_{\text{ext}}) = 0$. The determination of the stable branch of the force-velocity relation is done by determining the intersection of the straight line of equation $(v_S + \tilde{F}_{\text{ext}}) = 0$ and of the force-velocity relation of equation $\tilde{F}_{\text{ext}} = v_S - \gamma v_S / (1 + 4\pi^2 v_S^2)$, *i.e.* by solving the equation

$$v_S - \gamma \frac{v_S}{1 + 4\pi^2 v_S^2 / \omega^2} = -v_S. \quad (\text{A.10})$$

The velocities that are smaller in absolute value than the solutions of this equation are on an unstable branch of the force-velocity relation. A part of the branch with positive slope is unstable as soon as $\xi_a / \xi > 8/3$.

Appendix A.3. Oscillations for localized rates

We present here one way of carrying out the linear analysis of the rigid two-state model for the localized rate approximation. The motor density is given by eq. (8)

$$\rho(x, t) = \int_0^\infty d\tau \omega_{\text{on}} e^{-\omega_{\text{on}}\tau - \int_0^\tau d\tau' \omega_{\text{off}}(x + X(t) - X(t - \tau'))}. \quad (\text{A.11})$$

Let us introduce $X(t) = F_{\text{stall}}/k + z(t)$. Expanding at first order in z , we obtain

$$\rho(x, t) = \int_0^\infty d\tau \omega_{\text{on}} e^{-\omega_{\text{on}}\tau - \omega_{\text{off}}(x)\tau} \times \left(1 - \int_0^\tau d\tau' \omega'_{\text{off}}(x) (z(t) - z(t - \tau')) \right). \quad (\text{A.12})$$

From this equation, we can deduce the motor force, which we also expand at linear order ($F_m = F_{\text{stall}} + f$)

$$f(t) = - \int_0^\infty d\tau N U \omega_{\text{on}} e^{-\omega_{\text{on}}\tau} \left(\frac{1 - e^{-\omega_{\text{off}}^{\text{max}}\tau}}{\tau a(1 - a)} \right) \times \int_0^\tau d\tau' (z(t) - z(t - \tau')). \quad (\text{A.13})$$

We expand z in series

$$z(t - \tau) = \sum_{n=0}^\infty z^{(n)}(t) \frac{(-\tau)^n}{n!}. \quad (\text{A.14})$$

Integration over the variable τ gives

$$f(t) = \sum_{n=1}^{\infty} \frac{NU\omega_{\text{on}}z^{(n)}(t)(-1)^{n+1}}{a(1-a)(n+1)} \left(\frac{1}{\omega_{\text{on}}^{n+1}} - \frac{1}{(\omega_{\text{on}} + \omega_{\text{off}}^{\text{max}})^{n+1}} \right). \quad (\text{A.15})$$

We take the Laplace transform

$$f(s) = z(s) \frac{N\omega_{\text{on}}U}{a(1-a)} \sum_{n=1}^{\infty} \frac{s^n(-1)^{n+1}}{n+1} \left(\frac{1}{\omega_{\text{on}}^{n+1}} - \frac{1}{(\omega_{\text{on}} + \omega_{\text{off}}^{\text{max}})^{n+1}} \right). \quad (\text{A.16})$$

We recognize a logarithm, which gives

$$f(s) = D(s)z(s), \quad (\text{A.17})$$

with:

$$D = \frac{N\omega_{\text{on}}U}{a(1-a)} \times \left[-\frac{1}{s} \ln \frac{1+s/\omega_{\text{on}}}{1+s/(\omega_{\text{on}} + \omega_{\text{off}}^{\text{max}})} + \frac{\omega_{\text{off}}^{\text{max}}}{\omega_{\text{on}}(\omega_{\text{on}} + \omega_{\text{off}}^{\text{max}})} \right]. \quad (\text{A.18})$$

The force balance equation $\xi \dot{z}(t) = -kz(t) + f(t)$ is written in Laplace variables as

$$(\xi s + k - D(s))z(s) = 0. \quad (\text{A.19})$$

The Hopf bifurcation is found by looking at the purely imaginary roots of $\xi s + k - D(s)$ of the type $s = iw$. We call $\alpha = \omega_{\text{off}}^{\text{max}}/\omega_{\text{on}}$ and set $\xi = \omega_{\text{on}} = 1$ (which fixes the units of time and energy). Inserting $s = iw$ into the equation $\xi s + k - D(s) = 0$ and separating real and imaginary parts lead to

$$k + \frac{NU}{a(1-a)} \left[-\frac{\alpha}{1+\alpha} + \frac{1}{w} \operatorname{atan} \left(\frac{\alpha w}{1+\alpha+w^2} \right) \right] = 0, \quad (\text{A.20})$$

$$-w + \frac{NU}{2a(1-a)w} \ln \frac{(1+\alpha+w^2)^2 + \alpha^2 w^2}{(1+\alpha)^2(1+w^2)^2} = 0. \quad (\text{A.21})$$

This system of equations defines the oscillation frequency $w/(2\pi)$ and the position of the threshold. For $k \rightarrow 0$, we find that condition to obtain oscillations is

$$\xi_a - \xi > O(k\omega_{\text{on}}^{-1}), \quad (\text{A.22})$$

where the effective friction is given by

$$\xi_a = \frac{NU\alpha(2+\alpha)}{2a(1-a)\omega_{\text{on}}(1+\alpha)^2}. \quad (\text{A.23})$$

It corresponds to the mean slope of the force-velocity relation at the origin if $\alpha \rightarrow \infty$. The period of the oscillations at threshold is given by

$$T_c = 2\pi \sqrt{\frac{2(3+3\alpha+\alpha^2)}{3(2+3\alpha+\alpha^2)}} \frac{\xi}{k\omega_{\text{on}}}. \quad (\text{A.24})$$

In the limit of large stiffnesses $k \rightarrow \infty$, we obtain

$$\xi_a > \frac{2+\alpha}{1+\alpha} k\omega_{\text{on}}^{-1}, \quad (\text{A.25})$$

$$T_c = 2\pi \sqrt{\frac{2\alpha}{(1+\alpha)\ln(1+\alpha^2)}} \frac{\xi}{k\omega_{\text{on}}}. \quad (\text{A.26})$$

For this choice of transition rates, the instability condition is still $\xi_a - \xi > kt_m$ (with a numerical coefficient that differs for low and large values of k), and the oscillation period is the geometrical mean of the times $t_m = \omega_{\text{on}}^{-1}$ and ξ/k .

Appendix A.4. Link between the age of contact τ and the elongation y

Here, we prove that eq. (38) that defines the crossbridge model by using the age of contact can be transformed to use the elongation y as a variable. Let us define the motor density $\rho_1(y, t)$ with elongation y at time t

$$\rho_1(y, t) = \int_0^{\infty} d\tau \rho(\tau, t) \delta(y - (y_0 + X(t) - X(t - \tau))). \quad (\text{A.27})$$

We note $\Psi = \Psi(y, t, \tau) = y - (y_0 + X(t) - X(t - \tau))$ and we compute the convective derivative of ρ_1

$$\begin{aligned} \partial_t \rho_1 + \partial_y \dot{X} \rho_1 &= \int_0^{\infty} d\tau (\partial_t + \dot{X}(t) \partial_y) \rho \delta(\Psi) \quad (\text{A.28}) \\ &= \int_0^{\infty} d\tau \left[(\partial_t \rho) \delta(\Psi) + \rho \delta'(\Psi) \dot{X}(t - \tau) \right]. \quad (\text{A.29}) \end{aligned}$$

We now replace $\partial_t \rho$ by its value for $\tau > 0$

$$\begin{aligned} \partial_t \rho_1 + \partial_y \dot{X} \rho_1 &= - \int_0^{\infty} d\tau \omega_{\text{off}} (y_0 + X(t) - X(t - \tau)) \rho \delta(\Psi) \\ &\quad - \int_0^{\infty} d\tau \left[(\partial_\tau \rho) \delta(\Psi) - \rho \delta'(\Psi) \dot{X}(t - \tau) \right]. \quad (\text{A.30}) \end{aligned}$$

We recognize a derivative in the second line and obtain

$$\partial_t \rho_1 + \partial_y \dot{X} \rho_1 = - \int_0^{\infty} d\tau [\omega_{\text{off}}(y) \rho \delta(\Psi) + \partial_\tau (\rho \delta(\Psi))]. \quad (\text{A.31})$$

Finally, we integrate by parts the term containing ∂_τ , and using the boundary condition $\rho(0, t) = \omega_{\text{on}}(1 - \int_0^{\infty} d\tau \rho)$, we obtain

$$\begin{aligned} \partial_t \rho_1 + \partial_y \dot{X} \rho_1 &= -\omega_{\text{off}}(y) \rho_1 \\ &\quad + \omega_{\text{on}} \delta(y - y_0) \left(1 - \int_{-\infty}^{\infty} dy' \rho_1(y', t) \right). \quad (\text{A.32}) \end{aligned}$$

This equation is exactly the conservation equation that one could have written directly with the variables y, t and shows the equivalence between the descriptions in terms of the two variables τ and y .

Appendix A.5. Linear analysis of the crossbridge model

Here, we describe how to carry out the linear analysis of the crossbridge model. Let us assume that $X(t) = F_{\text{stall}}/k + x(t)$, with $x(t)$ small compared to the length scale of variation of ω_{off} , and $\rho = \rho_S + \delta\rho$, with $\rho_S = \omega_{\text{on}}\omega_0/(\omega_{\text{on}} + \omega_0) \exp(-\omega_0\tau)$ the motor density at the stationary state. We define $\omega_0 = \omega_{\text{off}}(y_0)$ and $\alpha = \omega'_{\text{off}}(y_0)$. By developing at order 1 eq. (38), we obtain

$$\partial_t \delta\rho + \partial_\tau \delta\rho + \omega_0 \delta\rho + \alpha(x(t) - x(t-\tau))\rho_S(\tau) = 0, \quad (\text{A.33})$$

$$\delta\rho(0, \tau) = -\omega_{\text{on}} \int_0^\infty d\tau' \delta\rho. \quad (\text{A.34})$$

We integrate these equations over τ to obtain an equation for $\delta n(t) = \int_0^\infty d\tau \delta\rho$

$$\partial_t \delta n + (\omega_{\text{on}} + \omega_0)\delta n + \alpha \int_0^\infty d\tau (x(t) - x(t-\tau))\rho_S(\tau) = 0. \quad (\text{A.35})$$

We recognize a convolution product in the term on the right-hand side of this equation, which can therefore be simplified by taking the Laplace transform. Let us define $\delta n(s) = \int_0^\infty \delta n(t)e^{-st}$, we obtain

$$(s + \omega_{\text{on}} + \omega_0)\delta n(s) + \alpha \eta x(s) \frac{s}{s + \omega_0} = 0. \quad (\text{A.36})$$

We define $F_m = F_{\text{stall}} + f(t)$, then $f(t)$ satisfies the equation

$$f(t) = k_m N |y_0| \delta n - N k_m \int_0^\infty d\tau (x(t) - x(t-\tau))\rho_S. \quad (\text{A.37})$$

By taking the Laplace transform, we obtain

$$f(s) = k_m N |y_0| \delta n(s) - k_m N \eta x(s) \frac{s}{s + \omega_0}. \quad (\text{A.38})$$

If the position of the attachment point of the external spring is modified by δX_0 at $t = 0$, the force-balance equation in Laplace variables is written as

$$\xi s x(s) = -k(x(s) - \delta X_0/s) + f(s). \quad (\text{A.39})$$

Using the expressions for $f(s)$ and $\delta n(s)$, we obtain

$$x(s) = \frac{k \delta X_0 (s + \omega_0)(s + \omega_0 + \omega_{\text{on}})/s}{[(\xi s + k)(s + \omega_0) + k_m N \eta s](s + \omega_0 + \omega_{\text{on}}) - k_m N |y_0| \alpha \eta s}. \quad (\text{A.40})$$

The position of the instability threshold is found by looking at the purely imaginary poles $s = i\omega$ of this expression.

Appendix A.6. 3-state crossbridge model

Here, we describe the calculation of the active friction coefficient $\xi_a = \partial_v F_m|_{v=0}$ in the case of a 3-state crossbridge model. We call $\rho_i(\tau, t)$ the density of motors that are attached since a time τ and that are at time t in state i , and $n_d(t)$ the fraction of detached motors. We focus on the case where the filament velocity v is constant. The conservation of the motor number reads

$$\partial_\tau \rho_1 = -\omega_1(y_0 + v\tau)\rho_1, \quad \rho_1(0) = \omega_{\text{on}} n_d, \quad (\text{A.41})$$

$$\partial_\tau \rho_2 = \omega_1(y_0 + v\tau)\rho_1 - \omega_{\text{off}}\rho_2, \quad (\text{A.42})$$

$$n_d + \int_0^\infty d\tau (\rho_1 + \rho_2) = 1 \quad (\text{A.43})$$

$$F_m = -N k_m \int_0^\infty d\tau [(y_0 + v\tau)\rho_1 + (y_0 + d + v\tau)\rho_2]. \quad (\text{A.44})$$

Writing $\omega_1 = \omega_1(y_0) + \omega'_1(y_0)v\tau$, it is possible to obtain ρ_1 and ρ_2 analytically. After some calculations, we then find the following expression for the effective friction ξ_a :

$$\xi_a = \left(-1 + \frac{\alpha(-d\omega_{\text{on}} + y_0\omega_{\text{off}})}{G} \right) \times \frac{N k_m (\omega_1^2 + \omega_1\omega_{\text{off}} + \omega_{\text{off}}^2)\omega_{\text{on}}}{\omega_1\omega_{\text{off}}(\omega_{\text{off}}\omega_{\text{on}} + \omega_1(\omega_{\text{off}} + \omega_{\text{on}}))}, \quad (\text{A.45})$$

where we introduced $\omega_1 = \omega_1(y_0)$, $\alpha = \omega'_1(y_0)$, and

$$G = \frac{(\omega_1^2 + \omega_1\omega_{\text{off}} + \omega_{\text{off}}^2)(\omega_{\text{off}}\omega_{\text{on}} + \omega_1(\omega_{\text{off}} + \omega_{\text{on}}))}{\omega_{\text{off}}^2}. \quad (\text{A.46})$$

The value of ω_{on} for which $\xi_a = 0$ is simply found by solving the equation $G = \alpha(-d\omega_{\text{on}} + y_0\omega_{\text{off}})$. The result is given by eq. (56).

References

1. J. Howard, *Mechanics of Motor Proteins and the Cytoskeleton* (Sinauer Associates, Inc., Sunderland, 2001).
2. A. Fabiato, F. Fabiato, *J. Gen. Physiol.* **72**, 667 (1978).
3. D. Sasaki, H. Fujita, N. Fukuda, S. Kurihara, S. Ishiwata, *J. Muscle Res. Cell Motil.* **26**, 93 (2005).
4. D. Sasaki, N. Fukuda, S. Ishiwata, *Biochem. Biophys. Res. Commun.* **343**, 1146 (2006).
5. R.K. Josephson, J.G. Malamud, D.R. Stokes, *J. Exper. Biol.* **203**, 2713 (2000).
6. S. Camalet, F. Jülicher, J. Prost, *Phys. Rev. Lett.* **82**, 1590 (1999).
7. P. Martin, D. Bozovic, Y. Choe, A.J. Hudspeth, *J. Neurosci.* **23**, 4533 (2003).
8. S. Camalet, T. Duke, F. Jülicher, J. Prost, *Proc. Natl. Acad. Sci. U.S.A.* **97**, 3183 (2000).
9. M.A. Welte, *Curr. Biol.* **14**, R525 (2004).
10. S.P. Gross, M.A. Welte, S.M. Block, E.F. Wieschaus, *J. Cell. Biol.* **148**, 945 (2000).
11. M. Badoual, F. Jülicher, J. Prost, *Proc. Natl. Acad. Sci. U.S.A.* **99**, 6696 (2002).

12. F. Jülicher, J. Prost, Phys. Rev. Lett. **78**, 4510 (1997).
13. C.J. Brokaw, Proc. Natl. Acad. Sci. U.S.A. **72**, 3102 (1975).
14. A. Vilfan, E. Frey, F. Schwabl, Europhys. Lett. **45**, 283 (1999).
15. F. Jülicher, J. Prost, Phys. Rev. Lett. **75**, 2618 (1995).
16. M.J.I. Müller, S. Klumpp, R. Lipowsky, Proc. Natl. Acad. Sci. U.S.A. **105**, 4609 (2008).
17. A. Vilfan, E. Frey, J. Phys.: Condens. Matter **17**, S3901 (2005).
18. T. Guérin, J. Prost, P. Martin, J.-F. Joanny, Curr. Opin. Cell. Biol. **22**, 14 (2010).
19. J. Howard, Annu. Rev. Biophys. **38**, 217 (2009).
20. P.W. Anderson, Science **177**, 393 (1972).
21. D. Riveline, A. Ott, F. Jülicher, D.A. Winkelmann, O. Cardoso, J.J. Lacapère, S. Magnúsdóttir, J.L. Viovy, L. Gorre-Talini, J. Prost, Eur. Biophys. J. **27**, 403 (1998).
22. P.-Y. Plaçaïs, M. Baland, T. Guérin, J.-F. Joanny, P. Martin, Phys. Rev. Lett. **103**, 158102 (2009).
23. S. Günther, K. Kruse, New J. Phys. **9**, 417 (2007).
24. O. Campàs, P. Sens, Phys. Rev. Lett. **97**, 128102 (2006).
25. I.H. Riedel-Kruse, A. Hilfinger, J. Howard, F. Jülicher, Hum. Front. Sci. Prog. J. **1**, 192 (2007).
26. J. Pecreaux, J.-C. Roper, K. Kruse, J. Joanny, F. Jülicher, A.A. Hyman, S.W. Grill, J. Howard, Curr. Biol. **16**, 2111 (2006).
27. S.K. Vogel, N. Pavin, N. Maghelli, F. Jülicher, I.M. Tolic-Norrellykke, PLoS Biol. **7**, e1000087 (2009).
28. A.F. Huxley, Prog. Biophys. Biophys. Chem. **7**, 255 (1957).
29. T. Guérin, J. Prost, J.-F. Joanny, Phys. Rev. Lett. **104**, 248102 (2010).
30. D. Hexner, Y. Kafri, Phys. Biol. **6**, 036016 (2009).
31. T. Guérin, J. Prost, J.-F. Joanny, Phys. Rev. Lett. **106**, 068101 (2011).
32. W. Steffen, D. Smith, R. Simmons, J. Sleep, Proc. Natl. Acad. Sci. U.S.A. **98**, 14949 (2001).
33. B. Guirao, J.F. Joanny, Biophys. J. **92**, 1900 (2007).
34. F. Jülicher, A. Ajdari, J. Prost, Rev. Mod. Phys. **69**, 1269 (1997).
35. J.M. Carlson, A.A. Batista, Phys. Rev. E **53**, 4153 (1996).
36. B.N.J. Persson, *Sliding Friction: Physical Principles and Applications*, 2nd ed. (Springer, Heidelberg, 2000).
37. A.A. Batista, J.M. Carlson, Phys. Rev. E **57**, 4986 (1998).
38. S. Ishiwata, Y. Shimamoto, M. Suzuki, D. Sasaki, Adv. Exp. Med. Biol. **592**, 341 (2007).
39. T.A. Duke, Proc. Natl. Acad. Sci. U.S.A. **96**, 2770 (1999).
40. K.M. Gilmour, C.P. Ellington, J. Exp. Biol. **183**, 101 (1993).
41. D.M. Swank, V.K. Vishnudas, D.W. Maughan, Proc. Natl. Acad. Sci. U.S.A. **103**, 17543 (2006).
42. Y. Shimamoto, M. Suzuki, S. Ishiwata, Biochem. Biophys. Res. Commun. **366**, 233 (2008).
43. A. Huxley, R.M. Simmons, Nature **233**, 533 (1971).
44. P. Martin, A.D. Mehta, A.J. Hudspeth, Proc. Natl. Acad. Sci. U.S.A. **97**, 12026 (2000).
45. J.-Y. Tinevez, F. Jülicher, P. Martin, Biophys. J. **93**, 4053 (2007).
46. Y. Shimamoto, M. Suzuki, S.V. Mikhailenko, K. Yasuda, S. Ishiwata, Proc. Natl. Acad. Sci. U.S.A. **106**, 11954 (2009).
47. J. Murray, *Mathematical Biology*, second, corrected edition (Springer-verlag, Berlin, Heidelberg, 1993).
48. A. Vilfan, T. Duke, Biophys. J. **85**, 818 (2003).
49. H. Lacker, C. Peskin, in *Lectures on Mathematics in the Life Sciences*, Vol. **16**, edited by R.M. Muria (American Mathematical Society, 1986) p. 121.
50. T. Nishizaka, H. Miyata, H. Yoshikawa, S. Ishiwata, K. Kinoshita jr., Nature **377**, 251 (1995).
51. C. Veigel, J.E. Molloy, S. Schmitz, J. Kendrick-Jones, Nature Cell Biol. **5**, 980 (2003).
52. K. Tawada, K. Sekimoto, J. Theor. Biol. **150**, 193 (1991).
53. A. Schallamach, Wear **6**, 375 (1963).
54. G. Piazzesi, V. Lombardi, Biophys. J. **68**, 1966 (1995).
55. J.W. Pringle, Proc. R. Soc. London, Ser. B: Biol. Sci. **201**, 107 (1978).
56. K.B. Campbell, M. Chandra, J. Gen. Physiol. **127**, 89 (2006).
57. J.E. Stelzer, R.L. Moss, J. Gen. Physiol. **128**, 461 (2006).
58. M. Murase, H. Tanaka, K. Nishiyama, H. Shimizu, J. Muscle Res. Cell Motil. **7**, 2 (1986).
59. C.J. Brokaw, Biophys. J. **16**, 1029 (1976).
60. A. Lewalle, W. Steffen, O. Stevenson, Z. Ouyang, J. Sleep, Biophys. J. **94**, 2160 (2008).
61. J.M. Laakso, J.H. Lewis, H. Shuman, E.M. Ostap, Science **321**, 133 (2008).
62. M. Srinivasan, S. Walcott, Phys. Rev. E **80**, 046124 (2009).
63. V. Bormuth, V. Varga, J. Howard, E. Schäffer, Science **325**, 870 (2009).
64. W. Herzog, E.J. Lee, D.E. Rassier, J. Physiol. **574**, 635 (2006).
65. S. Grill, K. Kruse, F. Jülicher, Phys. Rev. Lett. **94**, 108104 (2006).